Vol. 47, No. 4 (2025) 768-791, DOI: 10.24874/ti.1951.05.25.09

Tribology in Industry

www.tribology.rs

RESEARCH

Enhancement of Steady-state Performance of Hydrodynamic Journal Bearings Using Macro-groove Textures with Lubricant Additives

Arun Bangotra[a,*], Sanjay Sharma[a]

[a]*School of Mechanical Engineering, Shri Mata Vaishno Devi University, Katra, India.*

Keywords:

Journal bearing
Macro-groove textures
Reynolds equation
Finite element method
Hydrodynamic lubrication
Load- carrying capacity
Friction coefficient
Lubricant additives

* Corresponding author:

Arun Bangotra
E-mail: arunbangotra@gmail.com

Received: 16 May 2025
Revised: 19 July 2025
Accepted: 13 September 2025

A B S T R A C T

The present study investigates numerically the steady-state performance of macro-grooved hydrodynamic journal bearings (MGHJB) with rectangular-shaped macro-grooves in different bearing surface regions, such as the full, first, second, and pressure-increasing regions. The steady-state parameters like load carrying capacity (LCC) and friction coefficient (FC) are calculated using the finite element approach by solving the governing Reynolds's equation of lubricant flow. The effect of rectangular macro-grooves provided in the specific regions of the journal bearing, along with the variation of groove depth and the area density, is considered for investigation at different eccentricity ratios. From the simulated results, the steady-state parameters of the journal bearing are enhanced from lower to higher eccentricity ratios. The maximum enhancement of LCC is 95.75% and reduction in friction coefficient (FC) is 48.67% found at the lower eccentricity ratio of 0.2 when four rectangular-shaped macro-grooves are provided in the pressure-increasing region at a groove depth of 0.9 and an area density of 58.50%. Furthermore, with the inclusion of 0.5% weight fractions of copper oxide and cerium oxide in the lubricant at 90°C, the steady-state performance of the bearing is further enhanced.

1. INTRODUCTION

In today's competitive technological development environment, the fundamental consideration while developing any machine component is its lifetime and dependability. A rotating shaft is always the key element of industry, such as electrical motors, generators, pumps, compressors, and high-speed machining spindles, etc. Bearings are used to guide and support shafts to minimize friction between components during relative movement. In mostly fast-speed rotational machinery, modifications to the surface topology of the bearing profile, such as surface waviness, texturing, grooves etc. as observed by different researchers, have an impact on the bearing's operation. Further, macro and micro texturing has been viewed as an

efficient means of lowering friction and increasing load-carrying capacity, especially at varying loads and speeds, and adds to enhanced efficiency, durability, and dependability of hydrodynamic journal bearings. To enhance the bearing performance, a designer must choose the appropriate texture distribution and its shape. The textured region acts as lubricant reservoir and enhances the nominal lubricant film thickness and minimizes the friction between two lubricating surfaces as textured or grooved area provides an enhanced clearance between journal and bearing surface thereby improving the performance of hydrodynamic journal bearing. Furthermore, several studies demonstrate that utilising lubricant additives including nanoparticles improves the overall efficiency and dependability of journal bearings. By incorporating appropriate texturing shape, optimum number of textures and nanoparticle additives in the base lubricants can be a promising approach for enhancing the steady-state performance of bearings in high-speed machines.

Many studies in past few years have investigated the impact of different geometrical characteristics such as texture/groove shape, size, and area density on the static and dynamic performance of journal bearings. C. C. Wang and C. L. He [1] reported that the herringbone grooves affected the performance of hydrodynamic journal bearing and the groove's tip produces the most pressure and can lower the outlet's average axial velocity. V. Kumar and S. C. Sharma [2] looked into the performance of hybrid thrust bearings with micro-grooves of trapezoidal, triangular, circular, and rectangular geometries. They discovered that rectangular grooves offer the highest load-carrying capacity at the optimum value for groove width and depth. Further many researchers have explored the effects of partial texturing on the bearing regions. M. Qiu et al. [3] investigated the effects of commonly used dimple forms on gas-lubricated slider bearings, and discovered that the maximum performances are achieved by using the ellipsoidal dimple. The effect of rectangular texture on the tribological performance of a journal bearing under steady-state condition was studied by authors [4], with a focus on its geometry by modifying the ratios and positions. The results showed that rectangular shaped micro-dimples can significantly increase journal bearing performance. N. Tala Ighil et al. [5] investigated the operation of textured journal bearings with spherical and cylindrical distributions. They determined that entire texture regions had a negative impact on journal bearing performance while partial texture regions had a positive effect. A star-like texture lowers the friction coefficient more than a triangle, circle, ellipse, or chevron shaped textures on the bearing surface [6]. Micro-grooving reduces the average temperature and enhance the friction coefficient when compared to spherical texture on hydrodynamic journal bearing [7]. S. Sharma et al. [8-9] used the finite element analysis to investigate the effect of protruded, triangular and chevron-shaped dimple texture on the hydrodynamic journal bearing and reported that load capacity enhances and friction coefficient reduces with an increase in the textured depth when it is located in an area of increasing pressure. The static characteristics of a bearing are enhanced when its dimples are located in its pressure-rising part and the load capacity is increased together with the friction force by the spikes at the pressure-falling zone [10]. Further, a well-chosen lubricant rheology, slip boundary condition, and micro-texture all work together to improve the hydrodynamic lubrication film stability in journal bearings [11]. The test findings by [12] revealed that textured surfaces significantly reduce wear in non-magnetic, brittle and plastic materials. However, this wear reduction effect is less noticeable in bearings polluted with magnetic compounds. P. Li et al. [13] investigated the impact of various bottom profiles of square textured bearings and reported that flat bottom yield maximum static performance of journal bearing. B. Jiao et al. [14] reported the enhancement of the load-carrying capacity, wear resistance, and coefficient of friction of tribo-pairs by using appropriate surface texture on two contact surfaces. They investigated the effect of texture characteristics such as the elliptical aspect ratio, depth-to-diameter ratio, density, and distribution on tribology performance. The results revealed that density had a significant impact on the coefficient of friction and load-carrying capacity. The fully spherical textured hybrid bearing has lower frictional torque in comparison to partial textured as reported by [15], while there is increased performance metrics of the cylindrical, spherical, triangle, and kite-textured bearings when the texture distribution occurs in the

bearing's pressure-rising zone [16]. The appropriate values for the depth, angle, circumferential width ratio, and number of grooves improved the bearing's load capacity, maximum film pressure, and energy efficiency [17]. Furthermore, it was discovered that groove radial width has the greatest influence on bearing performance differences under different rotation orientations, followed by the effects of the angle, number, circumferential width ratio, and depth of the groove. The characteristics of flexible bearing with texturing depend upon the number of textures, its depth and location [18], while, a partial texturing slider with orientation grooves parabolic with infinite width, the lubricant pressure depends upon the orientation angle of groove, density area and depth [19]. G. Xu et al. [20] by using the finite difference technique reported that the hybrid water-lubricated herringbone groove journal bearing has larger dynamic coefficients and better system stability in comparison with the hydrodynamic groove bearing at low speed, while at high speed hydrodynamic effect dominants the hydrostatic effect. A. B. Shinde and P. M. Pawar [21] determined the optimal configuration for journal bearings with partial micro-grooves. T. Chen et al. [22] determined the best geometrical parameters for the partially textured bearings with circular grooves to maximize their load-carrying capacity. In recent times, H. Feng et al. [23] analyzed the water-lubricated grooved hydrodynamic journal bearing and discovered that the groove texture parameters have an impact on the load capacity and significantly raise the load capacity at high rotational speed and less eccentricity ratio. By using numerical investigation [24] showed that the bearing system's stability and minimal fluid layer thickness are increased due to micro-grooves and magneto rheological fluid. D. Li et al. [25] investigated surface texture parameters and concluded that the chevron groove texture was best suited for high speed and low load situations. Further, studies by [26-29] revealed various other 3-dimensional irregularities, including the non-circularity of bearing, surface waviness, different texturing and the journal shapes influence the steady-state performance characteristics of the bearing.

Lubricant helps for smooth relative motion between two bearing surfaces and reduces wear and friction. According to researchers [30-33], adding nanoparticles such as nano diamonds, copper-oxide, aluminum oxide, tungsten oxide etc. to mineral, synthetic, and bio-based lubricant oil enhances the lubricant's viscosity, which enhances the bearing's performance. P. Zulhanafi et al. [34] examined the performance of the bio-based lubricant, palm mid olein (PMO), in journal bearing applications and reported enhancement in pressure and reduction in friction. Further, T. P. Gundarneeya and D. P. Vakharia [35] investigated the journal bearing performance using nanoparticle additions in the Avalon base oil and discovered enhanced load capacity and maximum pressure in contrast to the oil with no nanoparticles at different speeds. K. G. Binu et al. [36] examined the impact of nano-additives i.e TiO_2 in lubricants, and concluded that using lubricant additives increases bearing load capacity. Moreover, S. R. Suryawanshi and J. T. Pattiwar [37] added nanoparticles at different weight fractions in plain and elliptical journal bearings, and measured the shear viscosity of the particles using the Tribotester, they reported that the elliptical bearing outperformed the plain bearing. Nano-lubricant had natural ability to improve the antifriction/anti-wear qualities of the main lubricant [38]. Further, metal oxide nanoparticles have emerged as critical engineering materials in lubricating oils, and extensively used in bearings, gears, bushings, electrical connections etc. B. Bhattacharjee et al. [39] investigated the hydrostatic bearing operating with nano-additives using a modified Darcy's flow equation and discovered that the enhancement in performance due to presence of nano-additives in the lubricant. R. K. Dang et al. [40] examined the characteristics of elliptical bearings operating with copper-oxide and tungsten oxide nano-additives lubricants at different percentage concentration by weight (0.5-0.2), at different eccentricity ratios, and discovered a rise in load-carrying capacity (LCC) and minimum enhancement of oil temperature at higher concentrations of nano-additives. P. Khan et al. [41] evaluated the static Performance characteristics across a variety of eccentricity ratios and power law index. When nanoparticles are added to base lubricants, the findings reveal an increase in load bearing capacity, maximum pressure, and friction force compared to the base lubricant. K. S. Babu et al. [42] created the viscosity equation mathematically by examining the effects of zinc oxide (ZnO) and aluminum oxide (Al_2O_3) nanoparticle in lubricant using FEM to solve Reynolds's equation and found an

enhancement of journal bearing performance. S. B. Kalakada et al. [43] created an mathematical equation based on experiment results with SAE 15W40 oil with various nano-additives, including CuO, Al_2O_3, CeO_2, etc. at temperatures 30-90°C and weight concentration of nano-additives as 0-0.5 percent in lubricant and found that bearing performance had been improved. K. Prabhakaran Nair et al. [44] employed CuO, Al_2O_3, CeO_2 nanoparticles in oil to calculate temperature and pressure distribution journal bearing using modified Reynolds and energy equations and solving the equations using FEM and MATLAB code. They adopted an iterative approach to determine film thickness and computed load capacity, friction force, end leakage, and attitude angle with nano-lubricants in iso-viscous and thermo-viscous environments and found that load capacity and friction force increased in all circumstances. K. Yathish et al. [45] found enhancement in the load-carrying capacity (LCC) of hydrodynamic journal bearing with two-axial groove operated on nano-lubricant including TiO_2 nanoparticle additions. The size of the nanoparticles can also affect the tribological properties of friction surfaces [46-47]. Further, researchers [48-49] have reported numerical techniques using MATLAB for hydrodynamic journal bearings problems.

After a through literature review, it has been observed that the applications of micro-textures has gained popularity in tribological systems [50-51] during the last couple of decades, but notably, there is a lack of research specifically addressing the impact of macro-textured or grooved surfaces on the performance of journal bearing systems. More importantly, research gap exists in the limited exploration of macro-grooved regions such as the full region, first half, the second half region with most studies focusing primarily on the pressure-increasing region. Further investigation into these less-explored regions could provide a more comprehensive understanding of journal bearing performance. Further no study has yet been performed investigating the combined effects of rectangular macro-grooves situated in various regions of the bearing and the use of nanoparticle additives in lubricants on the steady-state performance parameters of hydrodynamic journal bearings. So, the objective of the present work aims to bridge this gap in the literature by providing critical insights into the interplay between rectangular macro-surface textures and lubricant additives and find the optimum design parameters. In this study, the effect of rectangular shaped macro-groove textures on the various regions of bearing surface, variation of groove numbers and depths, and area density is considered for investigation at the eccentricity ratios (0.2 to 0.8). Figure 1 (a) and (b) show the cross-sectional view and geometrical parameters of macro-grooved hydrodynamic journal bearing (MGHJB) considered in the present study. The results of this simulation study should help the designer for designing better hydrodynamic journal bearing that operates more smoothly and efficiently.

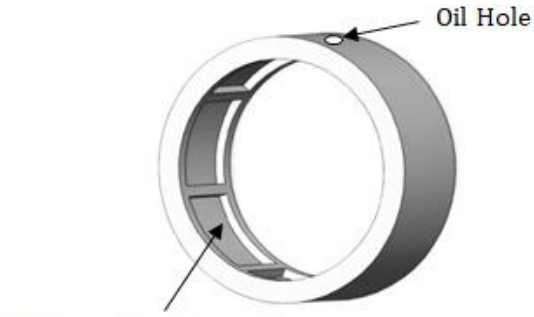

(a)

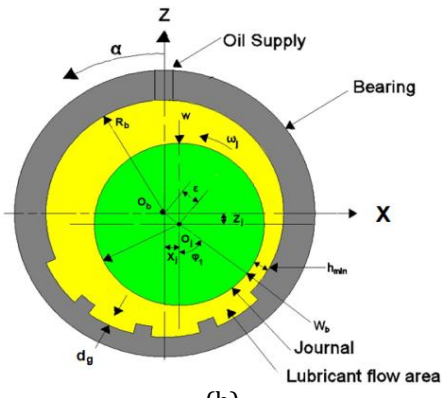

(b)

Fig 1. (a) Three-dimensional (b) Two-dimensional view of MGHJB with different coordinates.

2. MATHEMATICAL MODELLING

The governing non-dimensional form of Reynolds equation to determine the pressure distribution of thin viscous fluid layers for a journal bearing working at steady state regime, assuming that the flow is incompressible and laminar, Newtonian and iso-viscous fluid is written as [5,6]:

$$\frac{\partial}{\partial\alpha}\left[\bar{h}^3\bar{F}_2\left(\frac{\partial\bar{p}}{\partial\alpha}\right)\right]+\frac{\partial}{\partial\beta}\left[\bar{h}^3\bar{F}_2\left(\frac{\partial\bar{p}}{\partial\beta}\right)\right] =\bar{\Omega}\left[\frac{\partial}{\partial\alpha}\left\{\left(1-\frac{\bar{F}_1}{\bar{F}_0}\right)\bar{h}\right\}\right]+\frac{\partial\bar{h}}{\partial\bar{t}} \quad (1)$$

Where, $\bar{F}_0$, $\bar{F}_1$ and $\bar{F}_2$ are viscosities integrals are expressed as:

$$\bar{F}_0=\int_0^1\frac{1}{\bar{\mu}}d\,\bar{z},\quad \bar{F}_1=\int_0^1\frac{\bar{z}}{\bar{\mu}}d\,\bar{z}$$

$$\bar{F}_2=\int_0^1\frac{\bar{z}}{\bar{\mu}}\left(\bar{z}-\frac{\bar{F}_1}{\bar{F}_0}\right)d\,\bar{z}$$

In the present FEM-based Reynolds equation formulation, sharp-edge flow singularities and entry/exit losses along groove boundaries are not explicitly resolved, as the model assumes a smooth pressure variation within the lubricant film and neglects localized inertial effects. These singularities are inherently smoothed by the discretization process, and the governing equation does not capture abrupt velocity or pressure gradients that may occur in reality at - sharp edges. To minimize numerical artifacts, a sufficiently fine mesh has been used around groove boundaries to better approximate the pressure distribution. Additionally, the groove edge geometry in the model is idealized with a finite transition rather than an infinitely sharp corner, which helps reduce unrealistic singularities.

2.1 Lubricant- film thickness ($\bar{h}$)

The lubricant film thickness in non-dimensional form used in Equation (1) to determine the lubricant pressure distribution in the clearance space is expressed as [9]:

$$\bar{h}=(1-\bar{X}_j\cos\alpha-\bar{Z}_j\sin\alpha)+\bar{h}_g \quad (2)$$

Where, $\bar{X}_j$ and $\bar{Z}_j$ defines the steady-state journal centre co-ordinates, and $\bar{h}_g$ is the variation in lubricant-film thickness due to presence of the macro-groove in considered regions and can be expressed as [29]:

$$\bar{h}_g=0 \text{ if } (x_0,y_0)\notin\psi \text{ (For non-groove region)} \quad (3)$$

$$\bar{h}_g=\bar{d}_g \text{ if } (x_0,y_0)\in\psi \text{ (For rectangular macro-groove region)} \quad (4)$$

Where $\psi=\begin{Bmatrix}x_0\ge\alpha_b \text{ and } x_0\le\alpha_e\\ y_0\ge\beta_b \text{ and } y_0\le\beta_e\end{Bmatrix}$

x_0 and y_0 defines the local coordinates of the macro-groove. The two views of rectangular shaped macro-groove in shown in figure 2.

$\bar{d}_g$ = Non-dimensional depth of macro-groove

α_u = Unit cell angle for macro-groove

α_b = Starting angle of macro-groove = $0.125\alpha_u$

α_e = Ending angle of macro-groove = $0.875\alpha_u$

β_b , β_b = Macro - groove dimension in axial direction = ± 0.75

$\alpha=0-360^0$; for Full region;

$\alpha=0-180^0$; for 1st half region

$\alpha=180^0-360^0$; for 2nd half region;

$\alpha=144^0-288^0$; for pressure enhancing region

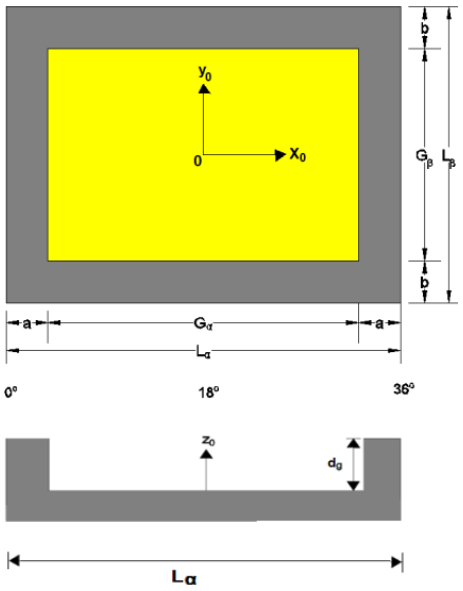

Fig. 2. Top View and Front view of rectangular macro - groove.

The macro-groove regions on bearing surface as mentioned above as defined in the equation (4) have been chosen from the pressure profile of the plain bearing and published literature [8,10] to place the rectangular macro-groove as depicted in figure 3 (a-d). One macro-groove length consists of 90°, 45°, and 36° in case of four rectangular macro-grooves placed in the full region, first or second half region and pressure-increasing region.

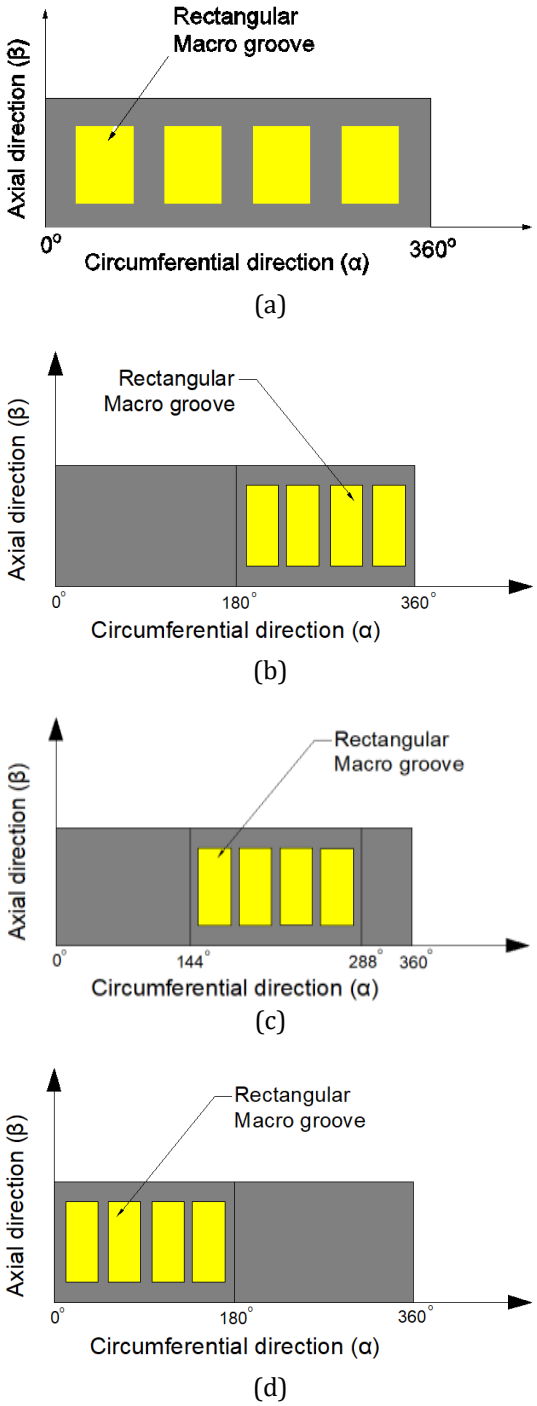

Fig. 3. Distribution of rectangular macro-groove on (a) Bearing full region (0–360^0); (b) First half region (0-180^0); (c) Second half region (180–360^0); (d) Pressure-enhancing region (144-288^0).

2.2 Finite element method

The non-dimensional Reynolds Equation (1) has been mathematically solved by using the finite element method. In order to discretize the lubricant flow domain, four nodded quadrilateral elements are used. The pressure is considered linearly distributed over an element along the two principal axis ζ and η is expressed as [48]:

$$\bar{p}_t = \sum_{j=1}^{n_e} N_j \bar{P}_j \;\; ; \;\; N_j = \frac{(1+\zeta_i\zeta)(1+\eta_i\eta)}{4} \tag{5}$$

Where, N_j is the shape factor of elements and n_e are the total number of nodes in each element.

By applying the Galerkin's FEM technique the weak formulation of Reynolds equation (1) has been is expressed as [48]:

$$\begin{aligned} &\frac{\partial}{\partial\alpha}\left[\bar{h}^3\bar{F}_2\frac{\partial}{\partial\alpha}\left(\sum_{j=1}^{4}N_j\bar{P}_j\right)\right] \\ &+\frac{\partial}{\partial\beta}\left[\bar{h}^3\bar{F}_2\frac{\partial}{\partial\beta}\left(\sum_{j=1}^{4}N_j\bar{P}_j\right)\right] \\ &-\bar{\Omega}\left[\frac{\partial}{\partial\alpha}\left\{\left(1-\frac{\bar{F}_1}{\bar{F}_0}\right)\bar{h}\right\}\right]-\frac{\partial\bar{h}}{\partial\bar{t}}=R^e \end{aligned} \tag{6}$$

In Galerkin's approach, the shape function of pressure, which is the primary variable, has been used as the weight itself. The above equation after simplification can be written in an algebraic equation in the matrix form expressed [6] as under:

$$\begin{aligned} &\sum_{e=1}^{n_e}\left[\left[\bar{F}_M\right]^e\left\{\bar{p}_V\right\}^e\right] \\ &=\sum_{e=1}^{n_e}\left[\begin{aligned}&\left\{\bar{Q}_V\right\}^e+\bar{\Omega}\left\{\bar{R}_H\right\}^e \\ &+\dot{\bar{X}}_j\left\{\bar{R}_{Xj}\right\}^e+\dot{\bar{Z}}_j\left\{\bar{R}_{Zj}\right\}^e\end{aligned}\right] \end{aligned} \tag{7}$$

For the eth element, for the Newtonian lubricant, the matrix and column vectors are expressed as:

$$\bar{F}^e_{Mij}=\int_{A^e}\int\left\{\frac{\bar{h}^3}{12\bar{\mu}}\left(\frac{\partial N_{Vi}}{\partial\alpha}\frac{\partial N_{Vj}}{\partial\alpha}+\frac{\partial N_{Vi}}{\partial\beta}\frac{\partial N_{Vj}}{\partial\beta}\right)\right\}d\alpha\,d\beta$$

$$\bar{Q}_{V_i}{}^e=\int_{\Gamma^e}\left\{\left(\frac{\bar{h}^3}{12\bar{\mu}}\frac{\partial\bar{p}_V}{\partial\alpha}-\frac{1}{2}\bar{\Omega}\bar{h}\right)n_1+\left(\frac{\bar{h}^3}{12\bar{\mu}}\frac{\partial\bar{p}_V}{\partial\beta}\right)n_2\right\}N_{Vi}d\bar{\Gamma}^e$$

$$\bar{R}^e_{Hi}=\int_{A^e}\int\frac{1}{2}\bar{h}\,\frac{\partial N_{Vi}}{\partial\alpha}\,d\alpha d\beta$$

$$\bar{R}^e_{Xji}=\int_{A^e}\int\cos\alpha N_{Vi}\,d\alpha d\beta$$

$$\bar{R}^e_{Xzi}=\int_{A^e}\int\sin\alpha N_{Vi}\,d\alpha d\beta$$

The directional cosines in each direction (α and β) are indicated by n_1 and n_2, while $i, j = 1, 2 \ldots n^e$.

2.3 Boundary conditions

The Boundary conditions used for the solution of the Reynolds equation are described as under [9]:

- On the two ends of the bearings i.e. at the leading edges, the value of the pressure is taken as atmospheric pressure.
- It is assumed that there is no pressure at nodes located on the external boundary of the bearing. $\bar{p}\,\big|_{\beta=\pm1} = 0.0$
- At the trailing edge of the positive zone, the boundary condition takes the impact of cavitation into account by assuming that the pressure gradient is zero: $\bar{p} = \dfrac{\partial \bar{p}}{\partial \alpha} = 0.0$

Equation (7) is solved to get the pressure and flow simultaneously because at each node one of the variables is known.

2.4 Viscosity equation

The non-dimensional viscosity equation [43], establishes a relation between (relative viscosity, $\bar{\mu}$), ϕ (percentage weight fraction of copper-oxide and cerium-oxide nano-additives in the reference base lubricant) and T (temperature), is used in the current analysis. The viscosity equation was formulated using the statistical method and experimental data with base lubricant (SAE 15W40 oil) with Copper oxide and Cerium oxide as nano-lubricant additives particles at a temperature of T = 30-90°C with a weight concentration range of ϕ = 0.1 - 0.5 percent in lubricant in non-dimensional form as under:

$$\bar{\mu} = \frac{\mu}{\mu_r} = e^{\left(K_1 - K_2\,\bar{T}\right)} \tag{8}$$

where, $\bar{T} = \dfrac{T}{T_{atm}}$

For CuO;

$K_1 = 1.142 - 1.126\phi + 5.120\,\phi^2 - 6.354\,\phi^3$
$K_2 = 1.163 - 1.041\,\phi + 4.218\,\phi^2 - 5.080\,\phi^3$

For CeO_2;

$K_1 = 1.142 - 0.311\phi + 1.377\,\phi^2 - 2.113\,\phi^3$
$K_2 = 1.163 - 0.431\,\phi + 1.521\,\phi^2 - 2.060\,\phi^3$

The relative viscosity, $\bar{\mu}$ is the ratio of nano-lubricant's viscosity at any temperature and the base lubricant's viscosity at similar temperature. Further, ϕ defines the percentage fraction by weight of nano-additives in the lubricant. The experimental findings demonstrate that the value of $\bar{\mu}$ with CuO and CeO_2 rises with an enhancement in the weight fraction of nano-additives and temperature [43]. In the current study, the different weight percentage of 0.1 - 0.5% of lubricant-additives particles (CuO and CeO_2) is used to compute values of $\bar{\mu}$ at 30°C, 60°C, and 90°C. By substituting the computed $\bar{\mu}$ at the specified temperature and the weight percentage of nanoparticles (ϕ) calculated using the aforementioned Eq. (8), the performance parameters of the macro-groove bearing has been computed using Reynolds equation and FEM.

2.5 Steady-state performance parameters

The dimensionless steady-state performance parameters of macro-grooved hydrodynamic journal bearing (MGHJB) are determined under static conditions i.e $\dot{\bar{X}}_j = \dot{\bar{Z}}_j = 0$. To determine the steady state parameters at a given vertical load ($\bar{W}$), the journal center equilibrium position need to be established.

Load-Carrying Capacity (LCC): The lubricant-film reaction components along X and Z directions respectively are written [15] as under:

$$\bar{W}_x = -\int_{-\lambda}^{\lambda}\int_{0}^{2\pi} \bar{p}\cos\alpha\, d\alpha\, d\beta \tag{9}$$

$$\bar{W}_z = -\int_{-\lambda}^{\lambda}\int_{0}^{2\pi} \bar{p}\sin\alpha\, d\alpha\, d\beta \tag{10}$$

The resultant fluid-film reaction i.e load-carrying capacity ($\bar{W}_b$) is expressed as [15]:

$$\therefore \bar{W}_b = \sqrt{\left(\bar{W}_x\right)^2 + \left(\bar{W}_z\right)^2} \tag{11}$$

Friction Coefficient (FC): The ratio of frictional force to load-carrying capacity (LCC) gives the friction coefficient (FC). The frictional force in the journal bearing is calculated using the following equation [15]:

$$\bar{F}_L = \sum_{e=1}^{n_e} \int_{A^e} \left(\Omega \frac{\bar{\tau}_c}{\bar{h}} + \frac{\bar{h}}{2} \frac{\partial \bar{p}}{\partial \alpha} \right) dA \qquad (12)$$

Where, $\bar{\tau}_c$ is the normalized couette shearing stress and is defined as $\bar{\tau}_c = 1 + (R_e)^{0.855}$

Where, $R_e = \frac{\rho U h}{\mu}$, and $\bar{\tau}_c$ = 1.0 in case of flow is laminar.

Friction coefficient (FC) of lubricant fluid film is calculated as under [16]:

$$\bar{f} = \frac{\bar{F}_L}{\bar{W}_b} \qquad (13)$$

3. SOLUTION PROCEDURE

A highly fine mesh of elements is necessary to get the accurate simulation's results. The accuracy of the solution and processing time both raise as the mesh density exceeds a particular value. Thus, to finalize the grid size, a mesh size testing is carried out before moving ahead. The calculation of load carrying capacity (LCC) for a rectangular macro-groove bearing with four macro-grooves, depth of 0.6 and eccentricity ratio 0.6 has been chosen under several mesh densities, as shown in Fig. 4. Initially, 200 (20 X10) elements as mesh density are selected to calculate LCC. However, above a certain level of improvement in value of LCC, the processing time increases significantly without a significant improvement in the accuracy of the result. The LCC of macro-grooved hydrodynamic journal-bearing (MGHJB) reach the desired level of precision with 1170 mesh density elements. Therefore, in the current theoretical investigation a mesh size of 65 × 18 elements is finalized to do necessary investigation. By using the overall solution procedure as shown in flow diagram in Fig. (5), the steady-state performance characteristics of macro-groove hydrodynamic journal bearing (MGHJB) were computed.

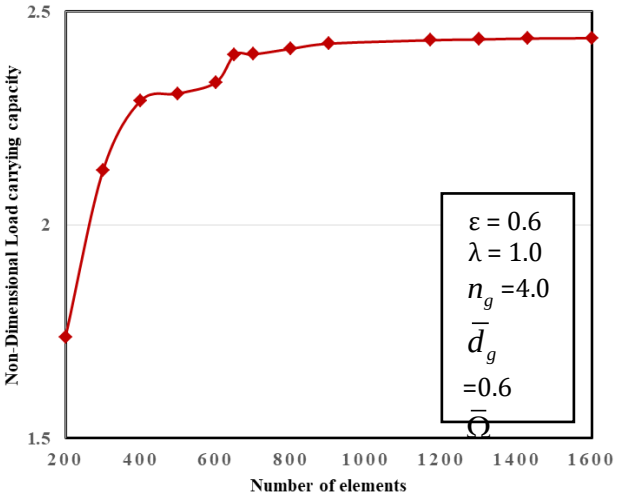

Fig. 4. Load-carrying capacity versus no. of elements to get optimal mesh size.

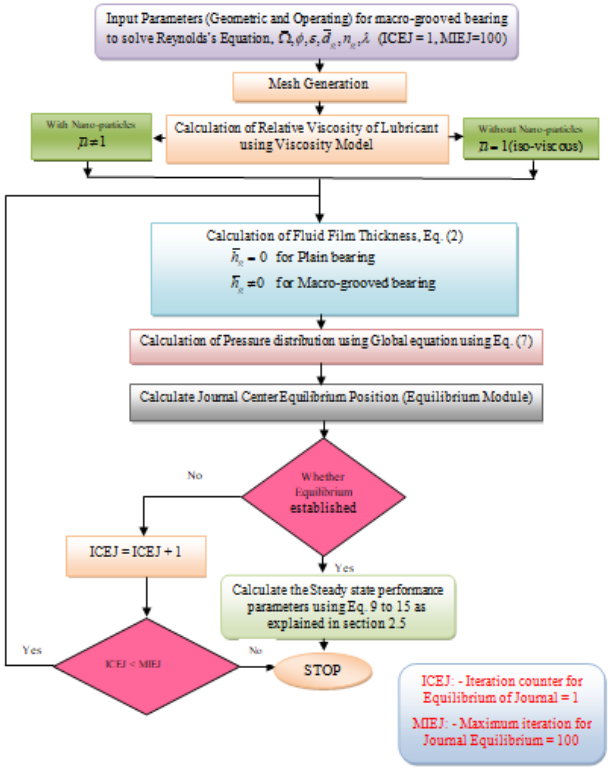

Fig. 5. Solution procedure flow chart.

The various dimensional and non-dimensional geometric and operating bearing input parameters are given in Table 1 [8, 43] used in the present study. Equation (1) is solved using the finite element analysis with the help of MATLAB program. To solve the system of equations in order to obtain the nodal pressure at every gauss point in the discretized fluid domain of lubricant, Gauss-Seidel methodology has been adopted. The subsequent prerequisites are tested for every node after calculating vector values $\{\bar{P}_0\}$ and $\{\bar{Q}\}$ from equation (7):

- Nodes are in the cavitation zone, $\{\bar{Q}\}$ <0;
- Nodes are in the lubricating flow zone, $\{\bar{P}_0\}$ > 0.

Table 1. Input parameters (operating and Geometric) for macro-grooved hydrodynamic journal bearing system [8,43].

Bearing Length	0.1 m
Journal radius	0.05 m
Bush external radius	0.055 m
Bush thickness	0.005 m
Radial clearance	5 X 10^{-5} m
Lub oil viscosity at 40^0C	0.0277 Ns/m^2
Lub oil density at 40^0C	860 kg/m^3
Inlet oil supply pressure	8.96 X 10^6 N/m^2
External Load	22.4 kN
Speed of journal	3000 rpm
Eccentricity ratio (ε)	0.2-0.8
No. of macro-grooves	1.0 – 4.0
Groove Depth ($\bar{d}_g$)	0.3-1.5
Aspect Ratio (λ)	1.0
Clearance Ratio ($\bar{C}$)	1.0
Speed characteristics ($\bar{\Omega}$)	1.0
No. of nodes	1235
Percentage weight fraction of nanoparticles in lubricants (ϕ)	0.1, 0.25, 0.5

Solutions will exist if these criteria are met; if not, nodes that don't fit the criteria will be moved to another region and the calculation process will keep going until a solution is found.

The computation is finished when Eq. (14), convergence criteria, is satisfied. The computations are carried out until the pressure differential at the subsequent iteration's node drops below the 0.1 percent limit.

$$\bar{Z}_0 = \left| \frac{\left[p_t^{-m'} \right] - \left[p_t^{-(m'-1)} \right]}{\left[p_t^{-(m'-1)} \right]} \right| \times 100 \leq TLM \quad (14)$$

Once the convergence criteria are satisfied, the steady-state performance parameters are determined using the equations as stated above.

4. RESULTS AND DISCUSSION

In this study, the steady-state static performance characteristics are determined for the smooth plain bearing and bearing with rectangular macro-grooves considering the different groove depth, groove number, and groove regions at the eccentricity ratios of 0.2 to 0.8 using the mesh size 65 ×18.

Before proceeding to numerical simulation, the validity of the FEM computed results from developed MATLAB codes from the present study is compared with already published results [8, 48, 49] for plain bearings as shown in Table 2. Moreover, the present results are also validated for plain bearing with published experimental result [51] as shown in Figure 6 and for journal bearing with different micro-textures with [9, 50] as shown in Table 3.

Table 2. MATLAB code validation with published data for plain bearing without nano-additives.

Eccentricity ratio = 0.7, Aspect Ratio=1.0 and Mesh density elements = 60*10				
Static parameters	**Current Study**	**S. Sharma et al. [8]**	**R.K Awasthi et al. [48]**	**H. N. Chandrawat and R. Sinhasan [49]**
LCC	8.03	8.04	7.44	7.98
Max Pressure	5.51	5.50	5.43	5.52
Film Thickness	0.30	0.33	0.30	0.30
FC	2.42	2.44	2.61	2.45
Attitude angle	44.89	44.84	45.22	44.97
Friction Power	19.57	19.58	19.40	19.57

Table 3. MATLAB code validation with published data for bearing with four number of textures, depth of 0.6 at eccentricity ratio of 0.2 and 0.6.

Static Parameters	**Eccentricity ratio**	**Current result**	**S. Sharma et al. [9]**	**D. Byotra and S. Sharma [50]**
LCC	0.2	1.337	1.377	1.386
	0.6	4.869	4.715	3.608
FC	0.2	8.930	9.561	9.339
	0.6	3.251	3.552	4.563

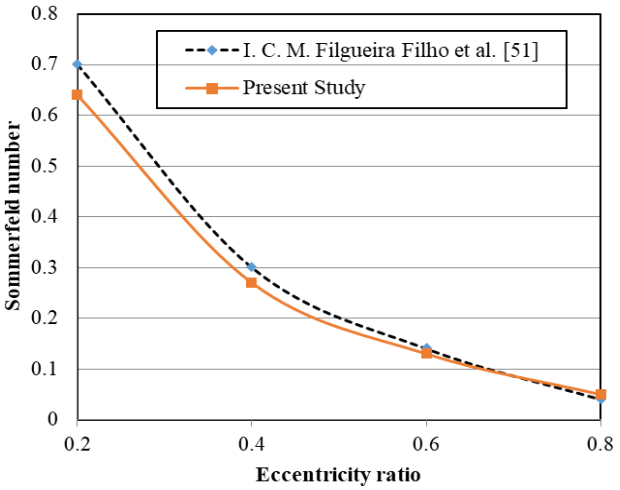

Fig. 6. Validation of present simulated result with experimental results of I.C.M Filgueira Filho et al. [51] for plain bearing.

The present results are found to be consistent with published results, thereby validating the MATLAB programme used in the current study and maximum difference of 5-8% has been observed. The difference in results may be due to different adopted numerical technique and mesh size.

The following regions [8] are selected on the bearing's circumferential direction for the placement of macro-grooves on the bearing surface as defined by equation (4) and shown in Fig. 3 (a-d):

a) Full Circumferential region (0°–360°)

b) First half region (0°–180°)

c) Second half region (180°–360°)

d) Pressure-increasing region (144°–288°

The pressure-increasing region (144°–288°) is considered highly effective in enhancing the load-carrying capacity (LCC) and reducing friction coefficient (FC) due to its favourable hydrodynamic conditions [8]. This is due to the fact that the lubricant pressure builds up in this region and has positive impact on bearing performance and hence this region is considered by various researchers for placement of textures. In present study the other regions i.e full circumferential area (0°–360°), first half region (0°–180°) and the second half region (180°- 360°) are also explored for deep understanding of various regions of the bearing for the placement of macro-groove textures. The number of rectangular macro-grooves placed in the circumferential direction of the bearing in different regions are taken as n_g = 1.0 to 4.0 and the non-dimensional groove depth is taken as $\bar{d}_g$ = 0.3 to 1.5.

In case of full surface of the bearing (0°–360°) with four rectangular macro-grooves, the first groove will occupy location on the bearing surface from 0°–90°, and then second will occupy 90°–180°, after that third groove will lie in 180° to 270° and finally fourth groove will lie in 270° to 360°. Hence, the total length of the unit cell (L_α) in circumferential direction for one groove is (0°–90°) or 1.571 radians. The total dimensions in axial directions of the groove is considered as L_β (-1 to +1). As shown in Fig. 2, the dimension 'a' and 'b' has been set as margins in the circumferential and axial directions respectively for placing the macro-groove and its values are taken initially as 12.5% of L_α and 12.5% of L_β. Hence the groove length in the circumferential direction (G_α) is initially taken as 75% of the cell dimension (L_α) and Groove width (G_β) is taken as 75% of the cell dimension (L_β) in the axial direction in different regions. Each rectangular groove is located in the bearing surface with a flat bottom surface. In the similar pattern the rectangular macro-groove textures are placed in the other regions also. The ratio of the area covered by the macro-groove texture to the entire area where the texture/groove is applied may be used to compute the groove area density (A_d), using the following equation:

$$A_d = \frac{\text{Area acquired by the macro-groove/texture}}{\text{Total area considered for groove/texture formation}} \times 100$$

In the present study, the eccentricity ratio has been restricted to a maximum value of 0.8 to avoid the onset of metal-to-metal contact. This criterion is based on the minimum film thickness calculated from the hydrodynamic analysis. For an eccentricity ratio approaching 1.0, the minimum film thickness tends toward zero, significantly increasing the risk of asperity contact between the journal and the bearing surface. By limiting the eccentricity ratio to 0.8, the analysis ensures that the lubricant film remains sufficiently thick to maintain full-film hydrodynamic lubrication, thus preventing metal-to-metal interaction. The steady-state parameters like load carrying capacity (LCC), friction coefficient (FC) of journal bearing are determined by considering rectangular macro-grooves in various regions. The whole analysis is performed at lower and higher ranges of eccentricity ratios and various groove numbers and depths and results are shown in Table 4 and 5 and Fig. 7-10. The main findings of this study for various regions are as under:

4.1 Full macro-groove region in circumferential direction (0°-360°)

Table 4 shows the static performance parameters of bearing with macro-grooves in various regions of bearing at eccentricity ratios, ε = 0.2 and 0.4, while Table 5 shows the static parameters at eccentricity ratios, ε = 0.6 and 0.8 respectively. It is observed that for rectangular macro-grooves distribution in the full region of bearing, the load-carrying capacity (LCC) is reduced at various groove numbers, depths, and eccentricity ratios, while friction coefficient (FC) is enhanced in comparison with the plain journal bearing. Therefore providing macro-groove textures in full region has a negative effect on the static parameters of the bearing. The most optimistic outcome were found with placement of one rectangular macro-groove i.e n_g =1.0, non-dimensional depth of groove, $\bar{d}_g$ = 1.5, and eccentricity ratio of 0.2, where LCC enhances by 5.25% and FC reduces by 1.35%, while most adverse impact were found at n_g = 1.0, $\bar{d}_g$ = 1.5, and higher eccentricity ratio, ε = 0.8, where LCC reduces by 5.34% and FC increases by 1.39% in comparison with plain bearing. It was further observed that the most adverse effect of full macro-grooved bearing was found at a higher eccentricity ratio. The drop in LCC and rise in FC due to the presence of macro-grooves on the bearing surface in this region may cause the flow rate to increase, it reduces the pressure generation and increasing the film thickness in the clearance gap, thereby reducing the static performance parameters.

4.2 Macro-grooves in first half region (0°-180°)

For rectangular macro-grooves distribution in the first half region of bearing, it was found from Table 4 and Table 5 that this configuration has also the detrimental effect on the LCC and FC for different values of groove numbers, depths, operating under different values of eccentricity ratios. The most optimistic results for this type of configuration were found at n_g = 1.0, $\bar{d}_g$ = 0.3, and eccentricity ratio of 0.2, where LCC reduces by 5.63% and FC increase by 5.87%, while detrimental outcomes were found at n_g = 2.0, $\bar{d}_g$ = 1.5, and eccentricity ratio of 0.2, where LCC reduces by 81.63% and FC increases by 49.49% in comparison with plain bearing. Further at average and higher eccentricity ratio of 0.6 and 0.8, it was observed that the LCC enhances while FC reduces at n_g = 3.0, $\bar{d}_g$ = 0.3 in the range of 1% in comparison with the plain bearing. It was further observed that the maximum reduction of performances was found at a lower eccentricity ratio at higher groove depth while the least reduction was found again at an average and high eccentricity ratio at lower groove depth.

Table 4. Static performance parameters of bearing with macro-grooves in various regions at ε=0.2 and 0.4.

Region	Groove numbe n_g	Groove Depth $\bar{d}_g$	Maximum Pressure ε = 0.2	Maximum Pressure ε = 0.4	LCC ε = 0.2	LCC ε = 0.4	FC ε = 0.2	FC ε = 0.4
Plain	0.0	0.0	0.482	1.273	1.013	2.430	12.763	5.823
0-360°	1.0	0.3	0.516	0.837	0.816	2.112	15.233	6.019
		0.6	0.523	0.858	0.754	2.205	18.232	6.520
		0.9	0.548	0.903	0.656	2.283	19.234	6.272
		1.2	0.503	0.873	0.623	2.305	21.323	6.259
		1.5	0.494	0.725	0.534	2.102	23.013	6.558
	2.0	0.3	0.528	0.967	0.618	1.951	20.817	7.154
		0.6	0.531	0.877	0.625	1.029	23.181	13.379
		0.9	0.498	1.046	0.727	1.206	25.516	18.879
		1.2	0.462	0.913	0.340	0.650	27.699	21.087
		1.5	0.454	0.907	0.293	0.598	31.345	23.234
	3.0	0.3	0.535	0.798	0.683	1.610	18.853	8.664
		0.6	0.715	0.957	0.634	1.152	20.300	12.026
		0.9	0.777	1.020	0.586	1.185	21.949	12.096
		1.2	0.775	1.006	0.527	1.633	24.373	13.001
		1.5	0.745	0.957	0.477	0.956	26.951	14.436
	4.0	0.3	0.527	0.991	0.738	1.743	17.458	8.027
		0.6	0.659	1.030	0.654	1.426	19.675	9.763
		0.9	0.729	1.055	0.635	1.439	20.261	9.665
		1.2	0.723	1.007	0.610	1.347	21.398	10.316
		1.5	0.681	0.922	0.553	1.207	23.260	11.496

0-180°	1.0	0.3	0.488	1.283	0.956	2.408	13.512	5.882
		0.6	0.476	1.286	0.768	2.359	16.799	6.002
		0.9	0.469	1.284	0.798	2.245	16.678	5.998
		1.2	0.498	1.289	0.601	2.140	16.989	6.102
		1.5	0.471	1.278	0.561	2.137	17.002	6.501
	2.0	0.3	0.481	1.286	0.865	2.408	14.928	5.882
		0.6	0.473	1.291	0.522	2.306	17.653	6.135
		0.9	0.547	1.294	0.296	2.181	18.380	6.478
		1.2	0.586	1.295	0.187	2.090	18.663	6.751
		1.5	0.571	1.295	0.186	2.040	19.080	6.911
	3.0	0.3	0.482	1.283	0.860	2.417	15.008	5.857
		0.6	0.481	1.288	0.663	2.299	19.453	6.148
		0.9	0.477	1.290	0.548	2.193	19.517	6.437
		1.2	0.479	1.290	0.513	2.136	20.121	6.603
		1.5	0.480	1.289	0.505	2.112	25.480	6.675
	4.0	0.3	0.483	1.284	0.906	2.400	14.255	5.898
		0.6	0.476	1.290	0.742	2.308	17.376	6.126
		0.9	0.469	1.292	0.636	2.246	20.271	6.290
		1.2	0.467	1.408	0.592	2.410	21.768	5.938
		1.5	0.466	1.291	0.562	2.191	22.899	6.443
180-360°	1.0	0.3	0.360	0.833	0.784	1.822	13.438	7.638
		0.6	0.513	0.813	0.667	1.789	15.678	7.897
		0.9	0.478	0.834	0.586	1.712	16.789	8.019
		1.2	0.412	0.805	0.538	1.702	17.183	8.234
		1.5	0.357	0.765	0.501	1.689	17.897	8.445
	2.0	0.3	0.544	0.987	0.688	1.643	18.700	8.495
		0.6	0.731	1.094	0.842	1.531	15.257	9.080
		0.9	0.785	1.131	0.882	1.606	14.557	8.648
		1.2	0.765	1.212	0.798	1.578	16.203	8.767
		1.5	0.723	1.109	0.756	1.523	16.789	9.123
	3.0	0.3	0.482	1.135	0.736	1.824	17.490	7.682
		0.6	0.511	1.242	0.621	1.844	20.687	7.569
		0.9	0.549	1.236	0.665	1.824	19.295	7.635
		1.2	0.536	1.154	0.655	1.177	19.596	7.863
		1.5	0.503	1.059	0.622	1.698	20.610	8.198
	4.0	0.3	0.404	0.960	0.667	1.866	19.299	7.505
		0.6	0.374	0.860	0.496	1.622	25.914	8.588
		0.9	0.402	0.849	0.490	1.543	26.192	9.006
		1.2	0.409	0.815	0.494	1.493	25.988	9.301
		1.5	0.395	0.780	0.492	1.460	26.087	9.513
144-288°	1.0	0.3	0.769	1.634	1.329	2.708	9.744	5.235
		0.6	0.809	1.572	1.439	2.688	9.014	5.273
		0.9	0.761	1.415	1.445	2.579	8.974	5.493
		1.2	0.696	1.267	1.408	2.453	9.210	5.770
		1.5	0.635	1.156	1.355	2.331	9.565	6.064
	2.0	0.3	0.841	1.726	1.371	2.792	9.448	5.076
		0.6	0.936	1.713	1.514	2.811	8.562	5.041
		0.9	0.908	1.542	1.536	2.685	8.442	5.274
		1.2	0.839	1.369	1.496	2.526	8.665	5.600
		1.5	0.765	1.214	1.431	2.367	9.061	5.969
	3.0	0.3	0.753	1.589	1.355	2.737	9.558	5.180
		0.6	0.847	1.598	1.491	2.754	8.689	5.146
		0.9	0.843	1.483	1.531	2.647	8.568	5.349
		1.2	0.797	1.346	1.476	2.503	8.783	5.650
		1.5	0.738	1.220	1.412	2.356	9.177	5.992
	4.0	0.3	0.819	1.698	1.366	2.786	9.477	5.087
		0.6	0.944	1.735	1.437	2.854	8.930	4.963
		0.9	0.952	1.701	1.600	2.923	8.103	4.906
		1.2	0.909	1.458	1.595	2.638	8.132	5.364
		1.5	0.850	1.309	1.553	2.486	8.352	5.686

Table 5. Static performance parameters of bearing with macro-grooves in various regions at ε=0.6 and 0.8.

Region	Groove numbe n_g	Groove Depth $\bar{d}_g$	Maximum Pressure ε = 0.6	Maximum Pressure ε = 0.6	LCC ε = 0.6	LCC ε = 0.8	FC ε = 0.6	FC ε = 0.8
Plain	0.0	0.0	3.170	11.114	5.206	14.072	3.254	1.728
0-360°	1.0	0.3	1.769	6.212	4.504	11.307	4.024	2.010
		0.6	2.236	5.450	4.507	9.484	4.975	2.312
		0.9	2.136	5.009	4.377	8.529	4.043	2.562
		1.2	2.875	4.424	4.919	7.197	4.348	3.073
		1.5	2.405	3.408	4.131	5.270	5.006	4.232
	2.0	0.3	1.643	3.268	3.889	7.287	4.213	3.082
		0.6	1.434	2.216	2.778	5.224	5.763	4.150
		0.9	1.046	1.744	1.206	3.361	13.059	6.310
		1.2	1.027	1.198	1.002	1.493	15.688	14.046
		1.5	0.987	1.008	0.983	1.045	17.567	15.345
	3.0	0.3	1.192	2.618	3.022	5.741	5.400	3.896
		0.6	1.308	1.773	1.727	2.586	9.270	8.317
		0.9	1.362	1.802	1.713	2.505	9.327	8.553
		1.2	1.318	1.704	1.633	2.398	9.764	8.916
		1.5	1.234	1.578	1.488	2.214	10.703	9.642
	4.0	0.3	1.680	2.758	3.020	4.800	5.422	4.640
		0.6	1.602	2.591	2.433	4.017	6.661	5.466
		0.9	1.561	2.296	2.431	3.843	6.658	5.688
		1.2	1.411	1.979	2.245	3.472	7.193	6.271
		1.5	1.264	1.709	1.965	2.986	8.196	7.265
0-180°	1.0	0.3	3.183	11.124	5.187	14.050	3.269	1.732
		0.6	3.193	11.132	5.157	14.021	3.289	1.736
		0.9	3.191	11.123	5.152	14.001	3.296	1.741
		1.2	3.190	11.101	5.121	13.989	3.312	1.745
		1.5	3.189	11.096	5.110	13.965	3.332	1.748
	2.0	0.3	3.182	11.121	5.202	14.076	3.260	1.728
		0.6	3.190	11.117	5.162	14.044	3.285	1.731
		0.9	3.191	11.110	5.105	13.999	3.319	1.736
		1.2	3.187	11.100	5.038	13.946	3.359	1.740
		1.5	3.180	11.090	4.973	13.885	3.398	1.746
	3.0	0.3	3.178	11.119	5.196	14.038	3.262	1.732
		0.6	3.181	11.113	5.122	13.975	3.306	1.739
		0.9	3.180	11.103	5.032	13.911	3.360	1.745
		1.2	3.181	11.089	4.967	13.853	3.399	1.749
		1.5	3.181	11.076	4.933	13.811	3.420	1.753
	4.0	0.3	3.179	11.118	5.188	14.053	3.267	1.731
		0.6	3.181	11.111	5.133	13.999	3.299	1.736
		0.9	3.179	11.101	5.076	13.931	3.333	1.742
		1.2	3.179	11.089	5.035	13.877	3.357	1.747
		1.5	3.178	11.078	5.010	13.839	3.372	1.750
180-360°	1.0	0.3	1.602	3.244	3.817	7.246	4.283	3.096
		0.6	1.598	2.986	2.678	4.456	5.234	4.023
		0.9	1.501	2.312	2.302	3.234	5.890	4.123
		1.2	1.411	2.012	2.001	3.102	6.234	5.678
		1.5	1.123	1.976	1.987	2.789	6.487	6.302
	2.0	0.3	1.673	2.749	2.936	4.760	5.568	4.675
		0.6	1.636	2.604	2.464	4.032	6.574	5.445
		0.9	1.586	2.298	2.503	3.888	6.460	5.623
		1.2	1.465	2.123	2.345	3.789	6.678	5.823
		1.5	1.321	2.001	2.203	3.456	6.823	6.012
	3.0	0.3	2.335	6.736	3.380	7.772	4.891	2.989
		0.6	2.635	6.345	3.741	8.297	4.410	2.779
		0.9	2.437	4.978	3.634	7.178	4.525	3.173
		1.2	2.147	4.018	3.401	6.206	4.823	3.638
		1.5	1.845	3.363	3.069	5.296	5.333	4.234
	4.0	0.3	2.357	6.890	3.838	9.345	4.320	2.318
		0.6	2.248	6.330	3.698	9.174	4.446	2.478
		0.9	2.121	5.365	3.521	8.211	4.653	2.750
		1.2	1.934	4.701	3.337	7.498	4.901	2.999
		1.5	1.777	4.206	3.141	6.955	5.203	3.224
144-288°	1.0	0.3	3.684	11.126	5.458	13.775	3.094	1.737
		0.6	3.206	7.924	5.082	11.321	3.309	2.087
		0.9	2.740	6.203	4.679	9.826	3.581	2.381
		1.2	2.387	5.271	4.341	8.868	3.847	2.618
		1.5	2.138	4.818	4.071	8.250	4.090	2.799

	2.0	0.3	3.743	10.590	5.526	13.026	3.066	1.828
		0.6	3.262	6.937	5.101	9.945	3.932	2.352
		0.9	2.701	5.096	4.578	8.159	3.654	2.828
		1.2	2.259	4.410	4.128	7.123	4.035	3.209
		1.5	1.999	3.967	3.780	6.428	4.391	3.532
	3.0	0.3	3.513	10.364	5.351	12.590	3.156	1.889
		0.6	3.159	7.868	4.983	10.315	3.372	2.268
		0.9	2.729	6.336	4.541	8.808	3.682	2.624
		1.2	2.377	5.401	4.153	7.807	4.010	2.934
		1.5	2.112	4.969	3.833	7.106	4.330	3.202
	4.0	0.3	3.728	10.855	5.273	12.148	3.198	1.981
		0.6	3.337	7.326	4.969	10.150	3.251	2.305
		0.9	2.819	5.265	4.681	8.207	3.575	2.810
		1.2	2.370	4.442	4.219	7.036	3.949	3.244
		1.5	2.063	3.973	3.843	6.246	4.320	3.626

4.3 Macro-groove in second half region (180°-360°)

Due to the placement of groove textures in the second half region of bearing, the value of LCC decreases and FC increases in comparison with smooth plain bearing. Furthermore, it was noted that for all eccentricity ratio values, the presence of macro-grooves in first half region (0-180°) yield better results than the second half region (180-360°) and full region (0-360°) since the value of LCC for macro-grooves in first half region is higher than the value of LCC found for macro-grooves in second half and full region for different groove numbers and depths. The most optimistic results for this type of configuration were found at n_g = 2.0, $\bar{d}_g$ = 0.9, and ε = 0.2, where LCC reduces by 12.93% and FC increase by 14.06%, while maximum reduction in performance due to macro-grooves in this region was found at n_g = 2.0, $\bar{d}_g$ = 1.5, ε = 0.8, where LCC reduces by 72.37% and FC increases by 225.41% in comparison with plain bearing. Specifically, the reduction in LCC and increase in FC observed when macro-grooves are located in the diverging zone (full or second-half regions) is primarily due to the formation of a lubricant reservoir. In this configuration, the grooves in the diverging region allow more lubricant to accumulate, which increases the local film thickness but diminishes the hydrodynamic wedge effect. This reduction in pressure build-up lowers the LCC, while the thicker lubricant film increases viscous shear, thereby raising the FC compared to a smooth plain bearing.

4.4 Macro-groove in the pressure-increasing region (144°-288°)

Tables 4 and 5 and Fig. 7 to 10 shows the variation in LCC and FC at different eccentricity ratio with one to four number of macro-groove i.e n_g = 1.0 to 4.0 and non-dimensional groove depth of $\bar{d}_g$ = 0.3 to 1.5. Fig. 7 (a) and (b) shows the variation of LCC and FC with placement of one macro-groove (n_g = 1.0) in pressure-increasing region at different eccentricity ratio and groove depth. It is observed that with placement of one macro-groove in pressure-increasing region, the greatest improvement of LCC is 42.64%, while FC reduces by 29.68% at ε=0.2 and, groove depth, $\bar{d}_g$ = 0.9 in comparison with the plain bearing.

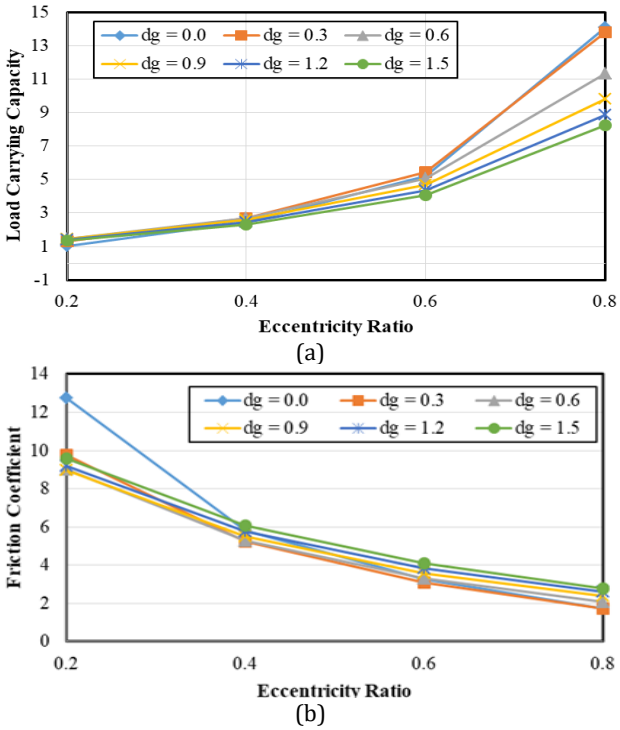

Fig. 7. (a) LCC versus eccentricity ratios (ε) (b) FC versus eccentricity ratios (ε) and groove depths for one macro-groove (n_g = 1.0) in pressure-increasing region.

Fig. 8 (a) and (b) shows that with two macro-grooves (n_g =2.0), the maximum enhancement of LCC is 51.62% and reduction in FC is 33.85% at ε=0.2 and, $\bar{d}_g$ = 0.9 in comparison with plain bearing.

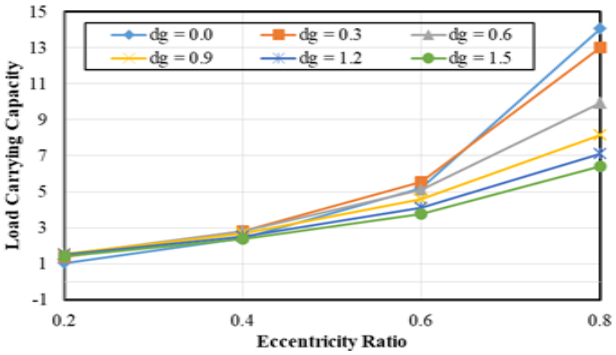

(a)

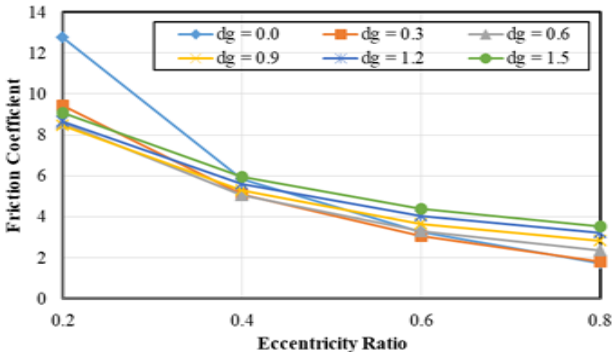

(b)

Fig. 8. (a) LCC versus eccentricity ratios (ε) (b) FC versus eccentricity ratios (ε) and groove depths for one macro-groove (n_g = 2.0) in pressure-increasing region.

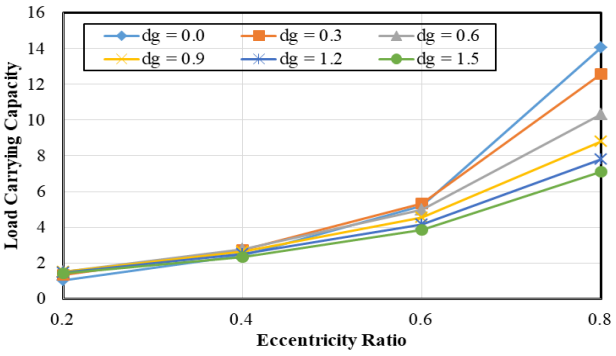

(a)

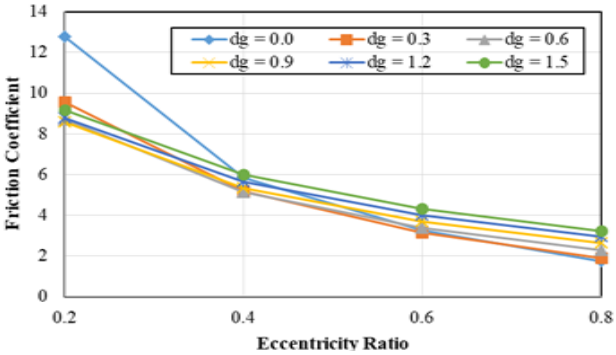

(b)

Fig. 9. (a) LCC versus eccentricity ratios (ε) (b) FC versus eccentricity ratios (ε) and groove depths for one macro-groove (n_g = 3.0) in pressure-increasing region.

Fig. 9 (a) and (b) depicts that with the placement of three macro-grooves (n_g = 3.0), the maximum increase in LCC is 49.35% while reduction in FC is 32.86% at ε=0.2 and, $\bar{d}_g$ = 0.9 in comparison with plain bearing.

While Fig. 10 (a) and (b) shows that due to the placement of four macro-grooves (n_g = 4.0) at ε=0.2 and, $\bar{d}_g$ = 0.9, LCC increases by 57.95% and FC reduces by 36.51%.

The reason for performance enhancement is that when macro-grooves are created in this region, a cavity is formed on account of which journal get an extra space in the clearance zone. As a result journal tries to move towards cavity formed due to macro-grooves and therefore the film thickness may reduce thereby increases the value of pressure and hence the LCC increases and FC decrease. At eccentricity ratio, ε=0.4, the value of LCC increases and FC decreases with increase in the groove number and depth and the maximum enhancement in LCC is 20.29% and reduction in FC is 15.75% at n_g = 4.0, $\bar{d}_g$ = 0.9 in comparison with the plain bearing.

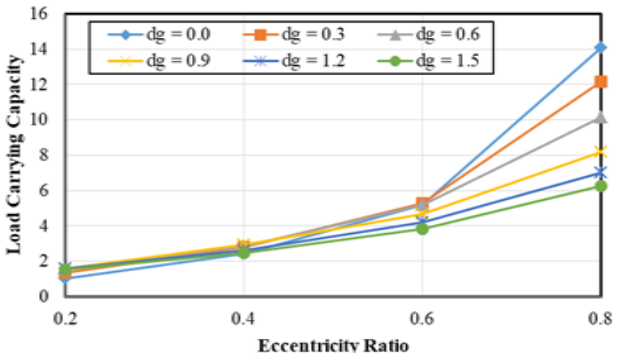

(a)

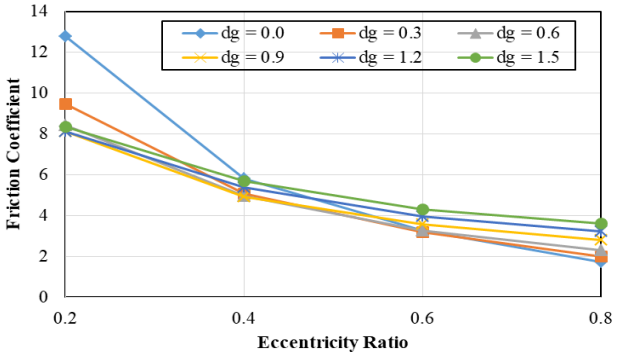

(b)

Fig. 10. (a) LCC versus eccentricity ratios (ε) (b) FC versus eccentricity ratios (ε) and groove depths for one macro-groove (n_g = 4.0) in pressure-increasing region.

It has been observed that at eccentricity ratio of 0.2, and 0.4 the LCC increases and FC decreases upon increasing the groove depth upto $\bar{d}_g$ = 0.9 and after that it shows the declining trend on any further increment in the value of depth of macro-groove. The results obtained at the low ratio of eccentricity of 0.2 and 0.4 established the significant effect on the performance of the bearing and confirm with the findings [8, 49]. At eccentricity ratio, ε=0.6, it was found that LCC decreases and FC increases with enhancement in groove number in this region, the maximum value of LCC and FC was found at low groove depth. At ε=0.6, the maximum enhancement in LCC is 6.15% and the reduction in FC is 5.77% at n_g = 2.0, $\bar{d}_g$ = 0.3. At higher eccentricity ratio, ε=0.8, the presence of macro grooves with different numbers and depths has negative effects on the performance of bearing. It is established that the performance is maximum at higher number of macro-groove at large value of the groove depth at low eccentricity ratio while by enhancing the eccentricity ratio the performance of bearing is found better only at lower number of macro-groove with low groove depth. The results further shows that positive effect of macro-groove on bearing performance are found with bearing operating at lower to average eccentricity ratios. The outcomes completely concur with the published findings [9].

4.5 Lubricant flow rate (Q)

In the present study, we had initially focused on global performance parameters such as load carrying capacity (LCC), and friction coefficient (FC) to assess the comparative performance of different configurations of rectangular shaped macro-grooves. The flow field distributions in the form of bearing lubricant flow rate diagrams are shown in Fig. 11 (a-d).

These provide additional physical insights into the pressure and velocity variations inside the bearing clearance, thereby complementing the global performance parameters presented in earlier sections. It has been found that geometrical discontinuities, such as macro-grooves, can create localized changes in the lubricant film thickness and pressure, which may disrupt the continuous flow and lead to increased flow resistance, although specific effects vary. The impact of these discontinuities depends on the geometry, number, and interaction with other factors like shaft speed, lubricant properties etc.

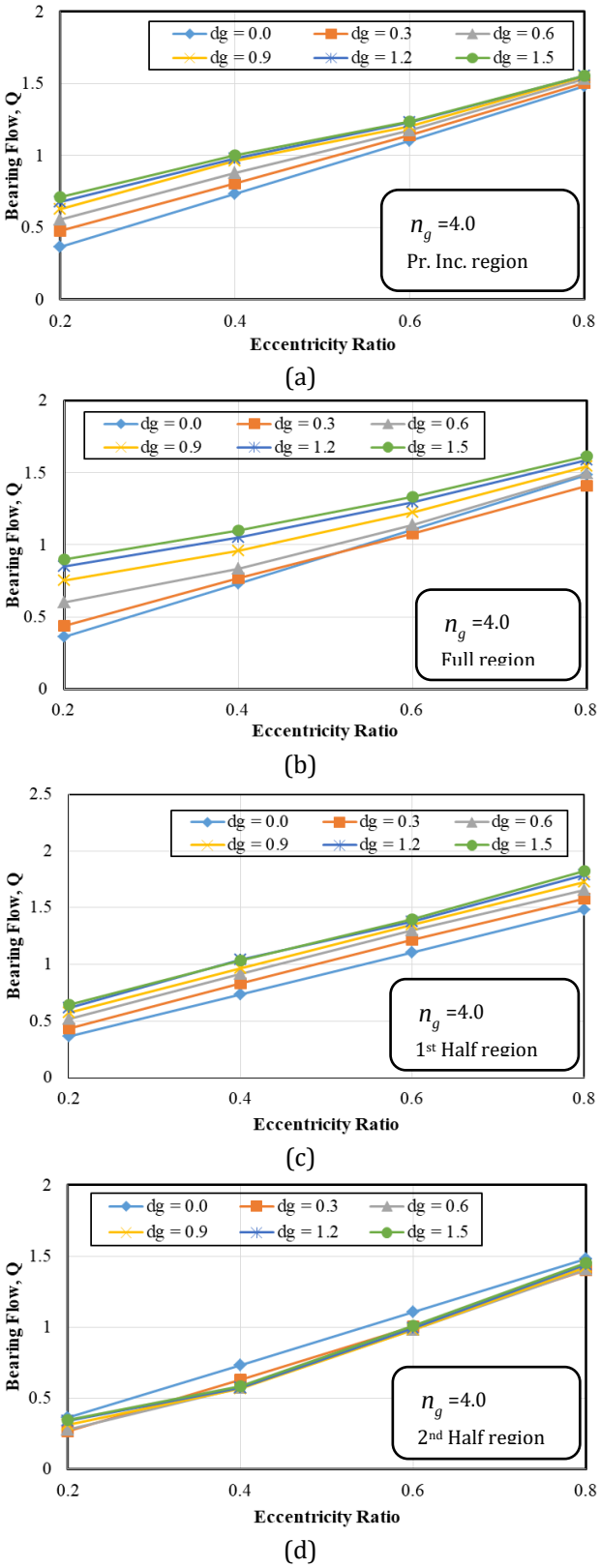

Fig. 11. (a-d) Bearing lubricant flow rate (Q) versus eccentricity ratios (ε) with four rectangular shaped macro-grooves (n_g = 4.0) and groove depths in different regions.

Fig 11 (a-d) depicts the non-dimensional bearing lubricant flow rate due to presence of four rectangular shaped macro-grooves in different regions of bearing surface. It has been found that maximum flow at eccentricity ratio of 0.2 and 0.4 is 146.03% and 50.14% respectively due to presence of four rectangular shaped macro-grooves in full region at n_g = 4.0, $\overline{d}_g$ = 1.5 in comparison with the plain bearing as shown in fig. 11 (b). While at eccentricity ratio of 0.6 and 0.8, the maximum lubricant flow rate is 26.82% and 23.12% respectively due to presence of four rectangular shaped macro-grooves in first half region at n_g = 4.0, $\overline{d}_g$ = 1.5 in comparison with the plain bearing as shown in fig. 11 (c).

4.6 Optimum parameters of rectangular macro-grooves in pressure increasing region (144°-288°)

After determining the maximum results in terms of load-carrying capacity (LCC) and friction coefficient (FC) due to presence of rectangular macro-grooves in the pressure-increasing region, further efforts were made to explore the potential performance by altering the area density by varying the dimensions of the rectangular macro-groove i.e G_α and G_β in pressure-increasing region. This has been done to examine whether area of the rectangular macro-groove could further affect the bearing's performance in pressure-increasing region where the pressure was higher, potentially leading to even better LCC and FC values. The groove length in the circumferential direction (G_α) is initially taken as 75% of the unit cell dimension (L_α) and Groove width (G_β) taken as 75% of the cell dimension (L_β) in the axial direction. The optimum parameters of rectangular macro-grooves have been determined at eccentricity ratio of 0.4. As found in earlier section 4.4 that with four rectangular shaped macro-grooves in the pressure-increasing region with depth, $\overline{d}_g$ = 0.9, at eccentricity ratio, ε=0.4 and area density of 56.25%, the maximum enhancement in LCC is 20.29% and reduction in FC is 15.75% in comparison with plain bearing.

The dimension of the rectangular macro-groove (G_α) in circumferential direction is varied by changing the value of margin 'a' along length of the unit cell, L_α as shown in Fig. 2. Corresponding to the maximum value of LCC, the optimum value of the groove length in the circumferential direction (G_α) is found as 90% of the cell dimension (L_α) i.e a=5% margin on both sides of the unit cell. Further by fixing the value of G_α and margin 'a', the margin in axial direction 'b' and Groove width (G_β) was varied and it was found that at G_β as 65% of the cell dimension (L_β) in the axial direction i.e b= 17.5% margin on both sides of the unit cell, the maximum value of LCC was found. Hence, it is established that with an area density of rectangular macro-groove as 58.50 %, there is enhancement of LCC as 27.78% and reduction in FC as 21.36% with four macro- grooves, n_g = 4.0, depth, $\overline{d}_g$ = 0.9, at eccentricity ratio, ε=0.4 in comparison with plain bearing. The outcomes corresponding to the optimal parameters of macro-groove agree with the published results [7]. With these optimum parameters and area density of 58.50 %, the performance of bearing in terms of LCC and FC was determined at eccentricity ratio 0.2 to 0.8. The maximum enhancement of LCC was found as 95.75% and reduction in COF as 48.67% at n_g = 4.0, $\overline{d}_g$ = 0.9 at ε=0.2, while at ε=0.6, n_g = 2.0, $\overline{d}_g$ = 0.3, LCC enhances by 7.96% and FC reduces by 6.84%. However, at higher eccentricity ratio of 0.8, the presence of macro-groove texture, the maximum performance was found at optimum geometry of one groove, n_g = 1.0 in pressure increasing region, at depth of 0.3, as LCC enhances by 1.72% and reduction in FC is 1.46%. The optimal dimensions of the four rectangular macro-grooves placed on the inner surface of bearing in terms of length, width and depth (in millimetre) at different eccentricity ratios (0.2 and 0.4) are 31.05 mm, 65 mm and 0.045 mm respectively. Hence, the optimal total length of the rectangular shaped macro-groove is 35.94% of the circumferential length of the bearing, while the total width of the groove is 65% of the axial length of the bearing.

Fig. 12 (a) - (b) shows a 3D surface plot of film thickness and pressure distribution as a function of the circumferential direction (α) and axial direction (β) for macro-grooves with four groove number, depth 0.3 and placed in full region.

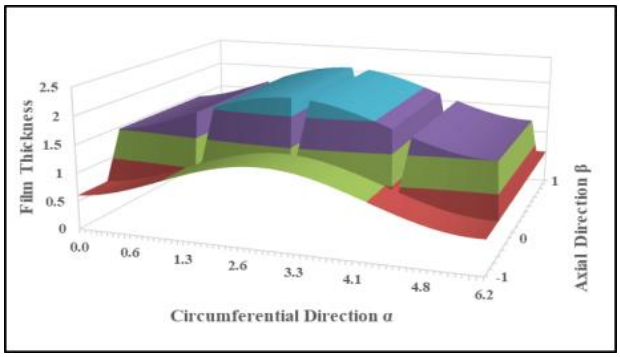

(a)

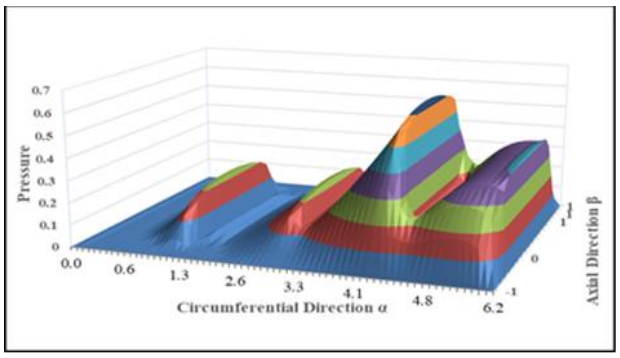

(b)

Fig. 12. (a) Non-dimensional Film thickness and (b) Pressure curve for bearing with four macro grooves in full region at groove depth, $\overline{d}_g$ = 0.3 at ε=0.2.

The pressure profiles illustrate how the pressure distribution varies across the bearing surface. This plot highlights areas of high and low pressure, which can help optimize performance, improve LCC and reduce FC in journal bearing. These variations are influenced by the groove number, depth, area density and region. Similarly the thickness profiles represent the film thickness across the bearing surface, crucial for maintaining lubrication and preventing metal to metal contact. These plots effectively highlight how the film thickness changes across these directions, pinpointing areas where the film is thinnest to ensure smooth operation.

4.7 Effect of lubricant additives on static performance parameters of macro-grooved hydrodynamic journal bearing (MGHJB)

Based on the previous studies and findings, this research focuses on improving the bearing's load-carrying capacity (LCC) and friction coefficient (FC) by incorporating nanoparticles as lubricant additives. It is observed that the performance of the journal bearing is improved with the addition of nanoparticles lubricant additives like CuO and CeO_2 in the lubricants. The inclusion of CuO and CeO_2 lubricant additives enhances lubricant viscosity [43]. The study is conducted at eccentricity ratio of 0.4 and aspect ratio of 1.0 using the optimal parameters of macro-grooved hydrodynamic journal bearing (MGHJB) determined in the earlier section to investigate the effect of further variations in static performance parameters using lubricant additives.

In the current study, LCC and FC of plain circular journal bearing operating with lubricant additives (CuO and CeO_2) is compared with macro-grooved hydrodynamic journal bearing (MGHJB) with four rectangular shaped macro-grooves in the pressure-enhancing region with optimum parameters as found earlier in section 4.6, with n_g = 4.0, depth, $\overline{d}_g$ = 0.9, at eccentricity ratio, ε = 0.4 with lubricant additives. The lubricant addtives as nanoparticles i.e copper-oxide (CuO) and cerium oxide (CeO_2) with percentage weight fraction, ϕ = 0.1 to 0.5% at different temperatures 30℃, 60℃, and 90℃ is considered. The calculated outcomes are depicted in Figure 13-14 that represents the value of LCC and FC of plain circular bearing and macro-grooved hydrodynamic journal bearing (MGHJB) with lubricant additives (CuO and CeO_2). The computed findings for plain circular bearing with nanoparticles with 0.5% weight fraction agree with published results [43].

Fig. 13 (a) shows the variation of LCC of plain bearing and macro-grooved hydrodynamic journal bearing (MGHJB) operating with lubricant additives with weight percentage as 0.1% at eccentricity ratio 0.4. It is found that for plain circular bearing there is an increase of LCC at an eccentricity ratio of 0.4 with 0.1% weight fraction of nanoparticles (ϕ = 0.1%) at a temperature of 90℃ with maximum enhancement of LCC is 13.05% for CuO and 8.02% for CeO_2 for plain bearing with lubricant additives in comparison with plain bearing operating without lubricant additives. Further for MGHJB with four macro-grooves in pressure-increasing region, n_g = 4.0, depth, $\overline{d}_g$ = 0.9 and ε=0.4, with ϕ = 0.1% lubricant additives at high temperature of 90℃, LCC increases by 44.16% for CuO and 37.78% for CeO_2 in comparison with plain bearing.

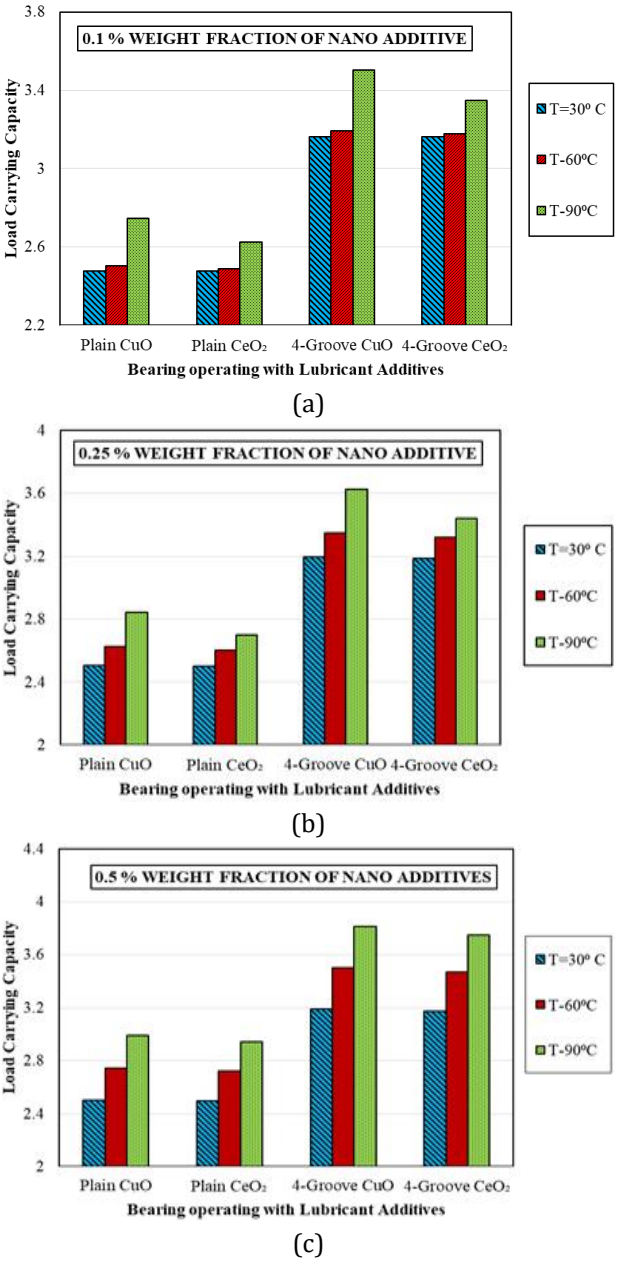

Fig. 13. (a), (b), and (c) LCC of plain and four macro-grooved bearing n_g = 4.0, $\bar{d}_g$ = 0.9 with lubricant additives ϕ = 0.1-0.5 % and eccentricity ratio 0.4.

Fig. 13 (b) shows the variation of LCC of plain bearing and MGHJB operating with lubricant additives with weight percentage as 0.25% at eccentricity ratio 0.4. It is found that plain bearing operating with ϕ=0.25% lubricant additives at the temperature of 90°C, LCC increases by 17.04% for CuO and 11.03% for CeO_2. For MGHJB with four macro-grooves, n_g = 4.0, depth, $\bar{d}_g$ = 0.9 and ε=0.4, and ϕ = 0.25% lubricant additives at 90°C, LCC increases by 49.26% for CuO and 41.61% for CeO_2. Fig. 13 (c) shows that for plain bearing operating with ϕ = 0.5% lubricant additives at the temperature of 90°C, LCC increases by 23.08% for CuO and 21.07% for CeO_2. For MGHJB with four macro-grooves, n_g = 4.0, depth, $\bar{d}_g$ = 0.9 and ε=0.4, and ϕ = 0.5% lubricant additives at 90°C, the maximum enhancement of LCC is 56.95% for CuO and 54.40% for CeO_2 in comparison with plain bearing operating without lubricant additives.

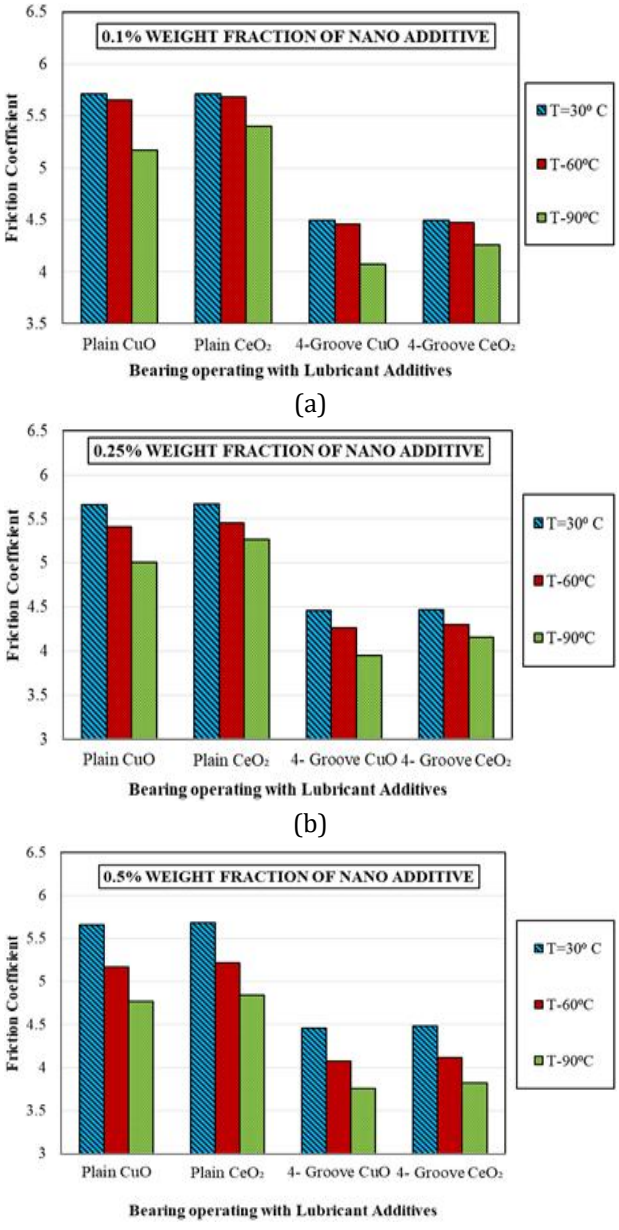

Fig. 14. (a), (b), and (c) FC of plain and four macro-grooved bearing n_g = 4.0, $\bar{d}_g$ = 0.9 with lubricant additives ϕ = 0.1-0.5 % and eccentricity ratio 0.4.

Fig. 14 (a) shows the variation of FC of plain bearing and MGHJB operating with lubricant additives with weight percentage as 0.1% at

eccentricity ratio 0.4. It is shown that FC reduces at ε=0.4, with ϕ = 0.1% lubricant additives at 90℃, with reduction of11.31% for CuO and 7.35% for CeO_2 for plain bearing and for MGHJB with four macro-grooves, n_g = 4.0, depth, $\overline{d}_g$ = 0.9 and ε=0.4 and ϕ = 0.1% lubricant additives at 90℃, FC reduces by 31.09% for CuO and 26.98% for CeO_2 in comparison with plain bearing.

With ϕ = 0.25% lubricant additives at 90℃ as shown in Fig. 14 (b) FC reduces by 14.25% for CuO and 9.77% for CeO_2 and for MGHJB with four macro-grooves, n_g = 4.0, depth, $\overline{d}_g$ = 0.9 and ε=0.4 with ϕ = 0.25% lubricant additives at 90℃, FC reduces by 32.38% for CuO and 28.89% for CeO_2.

Fig. 14 (c) shows that for plain bearing operating with ϕ = 0.5% lubricant additives at 90℃, COF reduces by 18.29% for CuO and 16.98% for CeO_2. For MGHJB with four macro-grooves, n_g = 4.0, depth, $\overline{d}_g$ = 0.9 and ε=0.4 with ϕ = 0.5% lubricant additives at 90℃, the maximum reduction is 35.45% for CuO and 34.54% for CeO_2 in comparison with plain bearing operating without lubricant additives. Hence it is established that presence of macro-grooves on the bearing inner surface and lubricant additives enhance the static performance in terms of LCC and FC of the bearing. The results agree with published work [30], which reported maximum performance of lubricant additives at high weight fraction and temperature.

The reason for increase in the LCC with nanoparticles addition is due to the increase in the value of relative viscosity. As the viscosity increases, the molecules in the lubricant may build chain like structure causes generation of more pressure leads to the enhancement of LCC. As per the literature [45], the size of the particles can also affect the performance. The key benefit of nanoparticles is their size within the nanometer scale (~ 10–120 nm), which is ideally suited for enhancement of tribological properties of friction surfaces or in other words minimizing the wear and tear loss between moving surfaces. These findings align with and expand upon the results of earlier research, demonstrating the potential of nanoparticle-enhanced lubricants to revolutionize the design and operation of journal bearing with macro-groove textures.

5. CONCLUSION

The static characteristics of the journal bearing considering the impact of rectangular macro-groove in the different regions and operating with lubricant additives CuO, and CeO_2 at temperatures of 30°C, 60°C, and 90°C with 0.1, 0.25 and 0.5 % concentrations is presented in the current research. The computed findings discussed in the aforementioned sections make the following evident conclusions:

- The presence of rectangular macro-grooves in the pressure-increasing region yielded the maximum steady-state parameters. At low eccentricity ratio 0.2, with four macro-grooves, and groove depth 0.9, with area density of 58.50%, the bearing's load-carrying capacity (LCC) increased by 95.75% and its friction coefficient (FC) reduced by 48.67%. When the eccentricity ratio is high, at 0.8, maximum performance was found with one macro-groove, at depth of 0.3, LCC enhances by 27.78% and FC reduces by 21.36 %.
- Further improvement of steady-state performance results from inclusion of nano-additives CuO and CeO_2 in base lubricant; at 90°C, the maximum improvement in LCC is 56.95% (CuO) and 54.40% (CeO_2), respectively, while the maximum reduction in FC is 35.45% (CuO) and 34.54% (CeO_2) with 0.5% concentrations of nanoparticles in lubricant compared to plain bearing operating without the nanoparticle lubricant additives. These findings emphasize the critical role of macro-grooves and nanoparticle additives in enhancing the steady-state performance of journal bearings, particularly under demanding operating conditions.
- Further investigation can be conducted by comparing the rectangular macro-groove texture presented in this study with various other geometries of the macro-grooves such as spherical, triangular, ellipsoidal, chevron etc. to potentially offer synergistic improvements in bearing performances. The research may be expanded further to evaluate the dynamic performance of bearings with macro-groove textures under transient conditions, encompassing start-up, shut-down, and changing load scenarios.

REFERENCES

[1] C.-C. Wang and C.-L. He, "Numerical study of a hydrodynamic journal bearing with herringbone grooves for oil leakage reduction," *Proceedings of the Institution of Mechanical Engineers Part J Journal of Engineering Tribology*, vol. 233, no. 3, pp. 439–446, Jun. 2018, doi: 10.1177/1350650118785660.

[2] V. Kumar and S. C. Sharma, "Effect of geometric shape of micro-grooves on the performance of textured hybrid thrust pad bearing," *Journal of the Brazilian Society of Mechanical Sciences and Engineering*, vol. 41, no. 11, Oct. 2019, doi: 10.1007/s40430-019-2016-0.

[3] M. Qiu, A. Delic, and B. Raeymaekers, "The effect of texture shape on the Load-Carrying capacity of Gas-Lubricated parallel slider bearings," *Tribology Letters*, vol. 48, no. 3, pp. 315–327, Aug. 2012, doi: 10.1007/s11249-012-0027-4.

[4] Y. A. Masmoudi, A. B. Chaouche, and A. Mokhtari, "Effect of rectangular rough dimples of textured surface on tribological behavior of a hydrodynamic journal bearing," *Tribology International*, vol. 189, p. 108945, Sep. 2023, doi: 10.1016/j.triboint.2023.108945.

[5] N. Tala-Ighil, M. Fillon, and P. Maspeyrot, "Effect of textured area on the performances of a hydrodynamic journal bearing," *Tribology International*, vol. 44, no. 3, pp. 211–219, Oct. 2010, doi: 10.1016/j.triboint.2010.10.003.

[6] M. S. Uddin and Y. W. Liu, "Design and optimization of a new geometric texture shape for the enhancement of hydrodynamic lubrication performance of parallel slider surfaces," *Biosurface and Biotribology*, vol. 2, no. 2, pp. 59–69, May 2016, doi: 10.1016/j.bsbt.2016.05.002.

[7] S. Kango, R. Sharma, and R. Pandey, "Comparative analysis of textured and grooved hydrodynamic journal bearing," *Proceedings of the Institution of Mechanical Engineers Part J Journal of Engineering Tribology*, vol. 228, no. 1, pp. 82–95, Aug. 2013, doi: 10.1177/1350650113499742.

[8] S. Sharma, A. Sharma, G. Jamwal, and R. K. Awasthi, "The effect of V-shape protruded and dimple textured on the load-carrying capacity and coefficient of friction of hydrodynamic journal bearing: A comparative numerical study," *Proceedings of the Institution of Mechanical Engineers Part J Journal of Engineering Tribology*, vol. 235, no. 5, pp. 997–1011, Jun. 2020, doi: 10.1177/1350650120935007.

[9] S. Sharma, A. Sharma, G. Jamwal, and R. K. Awasthi, "The effect of V-shape protruded and dimple textured on the load-carrying capacity and coefficient of friction of hydrodynamic journal bearing: A comparative numerical study," *Proceedings of the Institution of Mechanical Engineers Part J Journal of Engineering Tribology*, vol. 235, no. 5, pp. 997–1011, Jun. 2020, doi: 10.1177/1350650120935007.

[10] C. Gui and F. Meng, "Comparative study of spherical dimple and bump effects on the tribological performances of journal bearing," *Proceedings of the Institution of Mechanical Engineers Part J Journal of Engineering Tribology*, vol. 233, no. 1, pp. 139–157, Apr. 2018, doi: 10.1177/1350650118770355.

[11] M. Arif, S. Kango, and D. K. Shukla, "Analysis of textured journal bearing with slip boundary condition and pseudoplastic lubricants," *International Journal of Mechanical Sciences*, vol. 228, p. 107458, Jun. 2022, doi: 10.1016/j.ijmecsci.2022.107458.

[12] X. Zhao and Y. Zhang, "Analysis of the tribological and dynamic performance of textured bearings under contaminated conditions," *Tribology International*, vol. 187, p. 108732, Jun. 2023, doi: 10.1016/j.triboint.2023.108732.

[13] P. Li, F. Zeng, S. Xiao, D. Zhen, H. Zhang, and Z. Shi, "Effects of texture bottom profile on static and dynamic characteristics of journal bearings," *Shock and Vibration*, vol. 2021, no. 1, Jan. 2021, doi: 10.1155/2021/7068744.

[14] B. Jiao, Y. Liu, T. Li, X. Lu, and X. Ma, "Macro-texture in hydrodynamic lubrication: Effects of dimple parameter, density and distribution," *Proceedings of the Institution of Mechanical Engineers Part C Journal of Mechanical Engineering Science*, vol. 236, no. 15, pp. 8703–8713, Apr. 2022, doi: 10.1177/09544062221087552.

[15] C. B. Khatri and S. C. Sharma, "Influence of textured surface on the performance of non-recessed hybrid journal bearing operating with non-Newtonian lubricant," *Tribology International*, vol. 95, pp. 221–235, Dec. 2015, doi: 10.1016/j.triboint.2015.11.017.

[16] N. Singh and R. K. Awasthi, "Influence of texture geometries on the performance parameters of hydrodynamic journal bearing," *Proceedings of the Institution of Mechanical Engineers Part J Journal of Engineering Tribology*, vol. 235, no. 10, pp. 2056–2072, Jan. 2021, doi: 10.1177/1350650120982691.

[17] T. Ren and M. Feng, "Static Characteristics of a Micro Bidirectional Rotating Thrust Bearing with Novel Herringbone Grooves," *Lubricants*, vol. 13, no. 3, p. 109, Mar. 2025, doi: 10.3390/lubricants13030109.

[18] R. Yu, W. Chen, and P. Li, "The analysis of elastohydrodynamic lubrication in the textured journal bearing," *Proceedings of the Institution of Mechanical Engineers Part J Journal of Engineering Tribology*, vol. 230, no. 10, pp. 1197–1208, Jan. 2016, doi: 10.1177/1350650116630207.

[19] Y. Fu, J. Ji, and Q. Bi, "The Influence of Partially Textured Slider with Oriented Parabolic Grooves on the Behavior of Hydrodynamic Lubrication," *Tribology Transactions*, vol. 55, no. 2, pp. 210–217, Mar. 2012, doi: 10.1080/10402004.2011.643854.

[20] G. Xu, S. Jiang, C. Zhang, and X. Lin, "Dynamic characteristics of hybrid water-lubricated herringbone groove journal bearing," *Industrial Lubrication and Tribology*, vol. 77, no. 2, pp. 219–230, Dec. 2024, doi: 10.1108/ilt-06-2024-0233.

[21] A. B. Shinde and P. M. Pawar, "Effect of partial grooving on the performance of hydrodynamic journal bearing," *Industrial Lubrication and Tribology*, vol. 69, no. 4, pp. 574–584, Jun. 2017, doi: 10.1108/ilt-06-2016-0124.

[22] T. Chen, J. Ji, Y. Fu, P. Tian, J. Zhou, and X. Yang, "Tribological analysis of picosecond laser partially textured thrust bearings with circular grooves machined: Theory and experiment," *Proceedings of the Institution of Mechanical Engineers Part J Journal of Engineering Tribology*, vol. 236, no. 1, pp. 105–122, Mar. 2021, doi: 10.1177/13506501211005873.

[23] H. Feng, Z. Gao, Ron. A. J. Van Ostayen, and X. Zhang, "A numerical investigation of the effects of groove texture on the dynamics of a Water-Lubricated Bearing–Rotor system," *Lubricants*, vol. 11, no. 6, p. 242, May 2023, doi: 10.3390/lubricants11060242.

[24] S. C. Sharma and A. K. Tomar, "Study on MR fluid hybrid hole-entry spherical journal bearing with micro-grooves," *International Journal of Mechanical Sciences*, vol. 202–203, p. 106504, May 2021, doi: 10.1016/j.ijmecsci.2021.106504.

[25] D. Li *et al.*, "Theoretical analysis and experimental research of surface texture hydrodynamic lubrication," *Chinese Journal of Mechanical Engineering*, vol. 35, no. 1, Apr. 2022, doi: 10.1186/s10033-022-00691-7.

[26] K. Sahu and S. C. Sharma, "A study on performance of slot entry hybrid journal bearing considering effect of surface irregularities," *Industrial Lubrication and Tribology*, vol. 70, no. 6, pp. 1094–1109, Aug. 2018, doi: 10.1108/ilt-09-2017-0264.

[27] A. Bangotra and S. Sharma, "Impact of surface waviness on the static performance of journal bearing with CuO and CeO2 nanoparticles in the lubricant," *Industrial Lubrication and Tribology*, vol. 74, no. 7, pp. 853–867, Jun. 2022, doi: 10.1108/ilt-02-2022-0054.

[28] A. Bangotra and S. Sharma, "Impact of partial surface waviness on the tribological performance of hydrodynamic journal bearing," *Lubrication Science*, vol. 35, no. 3, pp. 207–224, Dec. 2022, doi: 10.1002/ls.1633.

[29] B. Manser, I. Belaidi, A. Hamrani, S. Khelladi, and F. Bakir, "Performance of hydrodynamic journal bearing under the combined influence of textured surface and journal misalignment: A numerical survey," *Comptes Rendus Mécanique*, vol. 347, no. 2, pp. 141–165, Jan. 2019, doi: 10.1016/j.crme.2018.11.002.

[30] J.-H. Lee *et al.*, "Effective viscosities and thermal conductivities of aqueous nanofluids containing low volume concentrations of Al2O3 nanoparticles," *International Journal of Heat and Mass Transfer*, vol. 51, no. 11–12, pp. 2651–2656, Jan. 2008, doi: 10.1016/j.ijheatmasstransfer.2007.10.026.

[31] W. Duangthongsuk and S. Wongwises, "Measurement of temperature-dependent thermal conductivity and viscosity of TiO2-water nanofluids," *Experimental Thermal and Fluid Science*, vol. 33, no. 4, pp. 706–714, Feb. 2009, doi: 10.1016/j.expthermflusci.2009.01.005.

[32] M. Kole and T. K. Dey, "Viscosity of alumina nanoparticles dispersed in car engine coolant," *Experimental Thermal and Fluid Science*, vol. 34, no. 6, pp. 677–683, Jan. 2010, doi: 10.1016/j.expthermflusci.2009.12.009.

[33] S. K. Mandal, B. Bhattacharjee, N. Biswas, K. Choudhuri, and P. Chakraborti, "Application of nanofluids on various performance characteristics of hydrodynamic journal bearing—A review," *Proceedings of the Institution of Mechanical Engineers Part E Journal of Process Mechanical Engineering*, vol. 236, no. 3, pp. 1229–1238, Dec. 2021, doi: 10.1177/09544089211063995.

[34] P. Zulhanafi, S. Syahrullail, and M. A. Ahmad, "The tribological performance of hydrodynamic journal bearing using bio-based lubricant," *Tribology in Industry*, vol. 42, no. 2, pp. 278–287, Jun. 2020, doi: 10.24874/ti.843.02.20.05.

[35] T. P. Gundarneeya and D. P. Vakharia, "Performance analysis of journal bearing operating on nanolubricants with TiO2, CuO and Al2O3 nanoparticles as lubricant additives," *Materials Today Proceedings*, vol. 45, pp. 5624–5630, Jan. 2021, doi: 10.1016/j.matpr.2021.02.350.

[36] K. G. Binu, B. S. Shenoy, D. S. Rao, and R. Pai, "Static characteristics of a fluid film bearing with TiO2 based nanolubricant using the modified Krieger–Dougherty viscosity model and couple stress model," *Tribology International*, vol. 75, pp. 69–79, Mar. 2014, doi: 10.1016/j.triboint.2014.03.013.

[37] S. R. Suryawanshi and J. T. Pattiwar, "Effect of TiO2 Nanoparticles Blended with Lubricating Oil on the Tribological Performance of the Journal Bearing," *Tribology in Industry*, vol. 40, no. 3, pp. 370–391, Sep. 2018, doi: 10.24874/ti.2018.40.03.04.

[38] A. Dhanola, "Chapter 7 Nanoengineered metal oxide additives as tribological performance modifiers," in *Machining and Tribology of Advanced Materials*, N. K. Singh, R. K. Verma, V. Kumar, and J. P. Davim, Eds., De Gruyter, 2025, pp. 125–138, doi: 10.1515/9783111377292-007.

[39] B. Bhattacharjee, P. Chakraborti, and K. Choudhuri, "Nano-fluid lubrication of single-layered porous hydrostatic bearing: a theoretical approach," *Journal of the Brazilian Society of Mechanical Sciences and Engineering*, vol. 42, no. 7, Jun. 2020, doi: 10.1007/s40430-020-02446-8.

[40] R. K. Dang, A. Chauhan, and S. Dhami, "Static thermal performance evaluation of elliptical journal bearings with nanolubricants," *Proceedings of the Institution of Mechanical Engineers Part J Journal of Engineering Tribology*, vol. 235, no. 8, pp. 1627–1640, Nov. 2020, doi: 10.1177/1350650120970742.

[41] P. Khan, A. Dhanola, and H. Garg, "Elasto-hydrodynamic analysis of journal bearing operating with nanolubricants," *Proceedings of the Institution of Mechanical Engineers Part J Journal of Engineering Tribology*, vol. 235, no. 5, pp. 963–974, Jun. 2020, doi: 10.1177/1350650120931979.

[42] K. S. Babu, K. P. Nair, and P. Rajendrakumar, "Computational analysis of journal bearing operating under lubricant containing Al2O3 and ZnO nanoparticles," *International Journal of Engineering Science and Technology*, vol. 6, no. 1, pp. 34–42, Feb. 2014, doi: 10.4314/ijest.v6i1.4.

[43] S. B. Kalakada, P. N. N. Kumarapillai, and R. K. P. K, "Static characteristics of thermohydrodynamic journal bearing operating under lubricants containing nanoparticles," *Industrial Lubrication and Tribology*, vol. 67, no. 1, pp. 38–46, Feb. 2015, doi: 10.1108/ilt-01-2013-0015.

[44] K. P. Nair, P. K. Rajendra Kumar, and K. S. Babu, "Thermohydrodynamic Analysis of Journal Bearing Operating Under Nanolubricants," in *ASME/STLE 2011 Joint Tribology Conference*, Los Angeles, California, USA: ASMEDC, Jan. 2011, pp. 17–21. doi: 10.1115/IJTC2011-61244.

[45] K. Yathish, K. G. Binu, R. S. D'Silva, S. B. Shenoy, and R. B. Pai, "Static characteristics of two-axial groove journal bearing operating on TiO_2 nanolubricant," *Journal of Mechanical Engineering and Automation*, vol. 5, no. 3B, pp. 94–99, 2015.

[46] W. Dai, B. Kheireddin, H. Gao, and H. Liang, "Roles of nanoparticles in oil lubrication," *Tribology International*, vol. 102, pp. 88–98, May 2016, doi: 10.1016/j.triboint.2016.05.020.

[47] T. Kulkarni, B. Toksha, and A. Autee, "Optimizing nanoparticle attributes for enhanced anti-wear performance in nano-lubricants," *Journal of Engineering and Applied Science*, vol. 71, no. 1, Feb. 2024, doi: 10.1186/s44147-024-00374-1.

[48] R. K. Awasthi, S. C. Jain, and S. C. Sharma, "Code development for the analysis of finite journal bearing system using MATLAB," in *Proceedings of the Fourth International Conference on Industrial Tribology*, Allied Publishers, India, pp. 501–507.

[49] H. N. Chandrawat and R. Sinhasan, "A comparison between two numerical techniques for hydrodynamic journal bearing problems," *Wear*, vol. 119, no. 1, pp. 77–87, Sep. 1987, doi: 10.1016/0043-1648(87)90099-8.

[50] D. Byotra and S. Sharma, "Performance analysis of textured journal bearing operating with and without nanoparticles in the lubricant," *Industrial Lubrication and Tribology*, vol. 74, no. 9, pp. 1028–1039, Aug. 2022, doi: 10.1108/ilt-03-2022-0078.

[51] I. C. M. F. Filho, A. C. Bottene, E. J. Silva, and R. Nicoletti, "Static behavior of plain journal bearings with textured journal - Experimental analysis," *Tribology International*, vol. 159, p. 106970, Mar. 2021, doi: 10.1016/j.triboint.2021.106970.

NOMENCLATURE

Dimensional parameters

c_r = Radial clearance, mm;
D_j = Diameter of Journal diamter, mm;
d_g = Macro-groove depth, mm;
e_j = Eccentricity of Journal, mm;
W_b = Load carrying capacity of bearing $(\partial h/\partial t \neq 0)$, N;
W_X, W_z = Load carrying capacity components $(\partial h/\partial t \neq 0)$, N;
F_L = Frictional Force, N;
t = time, sec;
h = fluid film thickness, mm;
h_g = variation in film thickness due to macro-groove, mm;
L_b = Length of Bearing, mm;
N_s = Speed (Rotational) of Journal, rpm;
p = Lubricant Pressure, N/mm^2;
p_s = Pressure of lubricant supply, N/mm^2 $(\mu_r \omega_j R_j^{\,2}/c_r^{\,2})$;
Q = Flow of lubricant, mm^3.sec^{-1}
R_j, R_b = Journal and bearing radius, mm;
W = Applied load on bearing, N;
x, y, z = Circumferential, Axial coordinates, and along film thickness, mm;
$X_j\ Z_j$ = Center coordinate of Journal, mm;

Greek Letters

μ = Lubricant viscosity Ns/m^2;
μ_r = Base reference lubricant viscosity Ns/m^2;
λ = Aspect ratio, (L_b/D_b)
ω_j = Journal speed, rad/s;
ϕ_1 = Attitude angle, rad;
$\bar{\Omega}$ = Speed parameter $(\omega_j \mu_r R_j^{\,2}/c_r^{\,2} p_{st})$

Non-Dimensional Parameters

$\bar{c}$ = c_r/R_j;
$\bar{F}_0, \bar{F}_1, \bar{F}_2$ = Viscosity functions;
$\bar{h}$ = h/c_r;
$\bar{h}_{\min}$ = $h_{\min}/c_r$;
$\bar{p}$ = p_t/p_s;
$\bar{t}$ = $tc_r^{\,2}p_s/\mu_r R_j^{\,2}$;
$\bar{W}$ = $W/p_s R_j^{\,2}$;
$\bar{W}_x, \bar{W}_z$ = $W_x/p_s R_j^{\,2}, W_z/p_s R_j^{\,2}$;
$\bar{X}_j, \bar{Z}_j$ = $X_j/c_r,\ Z_j/c_r$;
α, β = $x/R_j, y/R_j$;
$\bar{\mu}$ = μ/μ_r
$\bar{d}_g$ = d_g/c_r;
ε = Eccentricity ratio (e_j/c_r);
n_g = number of macro-groove;
$\bar{\Omega}$ = $\omega\ \mu_r R_j^{\,2}/c_r^{\,2} p_s$

Vectors and Matrices

$\left[\bar{F}_M\right]$ = Liquidity matrix;
$\left[\bar{N}_M\right]$ = Matrix for Shape function;
$\left\{\bar{p}_V\right\}$ = Vector for Nodal pressure;
$\left\{\bar{Q}_V\right\}$ = Vector for Nodal flow;
$\left\{\bar{R}_X, \bar{R}_Z\right\}$ = Vectors RHS due to center velocity of journal;
$\left\{\bar{R}_H\right\}$ = Hydrodynamic Column vector;